Contents lists available at SCCE

Journal of Soft Computing in Civil Engineering

Journal homepage: www.jsoftcivil.com

Structural Damage Detection Using Novel Objective Function and Hybrid Metaheuristic Algorithms

Soheil Sabzevari [1,*]; **Hosein Naderpour** [2]; **Majid Gholhaki** [2]

1. Ph.D. Candidate, Faculty of Civil Engineering, Semnan University, Semnan, Iran
2. Professor, Faculty of Civil Engineering, Semnan University, Semnan, Iran

* Corresponding author: *sabzevari.soheil@semnan.ac.ir*

https://doi.org/10.22115/SCCE.2025.2167

ARTICLE INFO

Article history:
Received: 30 August 2025
Revised: 28 September 2025
Accepted: 02 October 2025

Keywords:
Structural damage detection;
Model updating;
Novel objective function;
Optimization algorithm;
Hybrid algorithms;
Structural health monitoring.

ABSTRACT

Structural damage detection is vital for ensuring the safety, integrity, and serviceability of structures, which are inherently susceptible to progressive deterioration over time. This study presents an advanced model updating framework enhanced with metaheuristic optimization algorithms for accurate and robust identification of structural damage. A novel objective function was formulated by integrating three critical dynamic features: natural frequencies, mode shapes, and modal strain energy. To validate the effectiveness and robustness of the proposed approach, five metaheuristic algorithms—GOA, WOA, MRFO, SBOA, and AOA—were employed and their performance evaluated across two predefined damage scenarios under three levels of simulated noise (0%, 3%, and 10%). Comparative results indicated that while MRFO and SBOA achieved higher accuracy and noise resistance, GOA demonstrated faster convergence rates. To overcome limitations observed in individual algorithms, a novel hybrid optimization algorithm, MSOA, was developed. MSOA effectively balanced exploration and exploitation tendencies, improved convergence behavior, and reduced the risk of premature convergence, particularly under noisy conditions. The results demonstrate that the proposed model updating framework, which integrates a novel objective function with the MSOA algorithm, provides high accuracy and robustness for structural damage detection in frames, even in the presence of measurement uncertainty.

How to cite this article: Sabzevari S, Naderpour H, Gholhaki M. Structural damage detection using novel objective function and hybrid metaheuristic algorithms. Journal of Soft Computing in Civil Engineering. 2026;10(3):2167. https://doi.org/10.22115/scce.2025.2167

1. Introduction

Structural Health Monitoring (SHM) has emerged as a fundamental topic in civil engineering, aimed at ensuring the safety, durability, and functionality of structures throughout their service life. Structures are continuously exposed to environmental loads, operational effects, and degradation phenomena, while extreme events such as earthquakes can also cause severe damage. If such damages are not detected in a timely manner, they may pose significant risks to the performance and integrity of structures. Therefore, the development of accurate and reliable damage detection methods is essential, not only to prevent catastrophic failures but also to optimize maintenance strategies and reduce associated costs.

In recent years, approaches based on the dynamic characteristics of structures have received considerable attention. Modal parameters, due to their high sensitivity to stiffness variations caused by damage, have been widely employed as the basis for defining objective functions in damage detection. However, the use of each parameter individually is accompanied by inherent limitations; among the most significant drawbacks are the inability to accurately localize minor or distributed damages and the reduced accuracy under noisy conditions or when incomplete data are available. Afshar et al. [1] highlighted the growing role of ML and DL methods in SHM, demonstrating their potential to enhance accuracy and efficiency compared to conventional approaches. Similarly, Azimi et al. [2] presented a comprehensive review of deep learning approaches such as CNN and RNN for structural damage detection, discussing their requirements for large datasets and their sensitivity to noise.

In the process of damage detection, the design of the objective function plays a crucial role, as the accuracy and reliability of the results directly depend on its formulation. Since the use of individual dynamic parameters is associated with certain limitations, researchers have moved toward defining combined objective functions that simultaneously incorporate multiple indicators, thereby enhancing the sensitivity and robustness of the method. However, the optimization of such objective functions, due to the high dimensionality and computational complexity of the problem, requires advanced solution strategies. Consequently, metaheuristic algorithms have been extensively applied to explore the search space and obtain accurate solutions.

Over the past decade, a variety of nature-inspired metaheuristic algorithms have been introduced and applied in different engineering fields, including structural damage detection. The Grey Wolf Optimizer [3], inspired by the hunting behavior and social hierarchy of grey wolves, has been among the most widely used methods and has delivered remarkable results in various applications. The Ant Lion Optimizer [4], based on the predatory behavior of ant lions, and the Moth-Flame Optimizer [5], inspired by the navigation patterns of moths around light sources, have also been relatively popular and moderately utilized in recent years. Subsequently, the Whale Optimization Algorithm [6], developed from the bubble-net hunting strategy of humpback whales, became one of the most highly cited algorithms of the past decade owing to its fast convergence and strong performance. Afterward, the Satin Bowerbird Optimizer [7] was proposed, inspired by the mating and nesting behavior of satin bowerbirds; although innovative, its usage has remained limited compared to other algorithms. In the same year, the Grasshopper Optimization Algorithm [8] was developed by modeling the social interactions of grasshoppers and gained broader applications, particularly in damage detection, due to its balance between exploration and exploitation. More recently, the Manta Ray Foraging Optimization [9], simulating the foraging strategies of manta rays, has attracted significant attention for its ability to maintain population diversity and avoid local optima, rapidly establishing its place in the literature. Finally, the newer algorithms, namely the Secretary Bird Optimization Algorithm [10] inspired by the predatory behavior of secretary birds, and the Addax Optimization Algorithm [11] based on the foraging and burrowing behaviors of addaxes, have only recently been introduced; although still in their early stages of application, they demonstrate a growing trend of adoption in research.

Early studies on structural damage detection mainly focused on the use of single indicators or simple combinations of a limited number of dynamic features. For instance, Monteiro et al. [12] employed the WOA in a framework that relied solely on natural frequencies, which enabled damage detection but was limited in precise localization. Liu et al. [13] applied the grouped Modal Strain Energy (MSE) method for offshore platforms, achieving acceptable accuracy in axial damage detection, although the method was highly sensitive to environmental noise. Li et al. [14] proposed the covariance of dynamic strain responses (CoS) as a damage index, which allowed accurate identification of damage location and severity without the need for analytical models. Tan et al. [15] used the modal strain energy index to successfully detect both single and multiple damages in steel beams. In addition, Nabavi et al. [16] combined time-domain nodal accelerations with the GOA to effectively identify structural damage. Nouri et al. [17] proposed a vibration-based damage detection method using Fourier decomposition combined with ML algorithms, achieving high classification accuracy. Soleimani Nezhad et al. [18] investigated a two-story steel frame under seismic loading and employed Fourier and wavelet transforms to detect frequency reductions and locate damage. Fakharian and Naderpour [19] employed wavelet transforms and singular value decomposition for noise reduction and modal parameter extraction. Du et al. [20] developed a finite element model for panel zones in composite connections (CFSSTCs and steel–concrete beams), providing a precise constitutive model of shear performance validated by experiments. Khatir and Wahab [21] combined advanced finite element methods (XFEM and XIGA) with optimization algorithms (PSO and Jaya) for crack identification in plates, achieving improved convergence and accuracy, which was further validated experimentally.

Over time, it became evident that using a single indicator to design the objective function could not adequately address all damage scenarios, as each parameter carries its own inherent limitations. Consequently, researchers shifted toward combining multiple dynamic features to enhance the accuracy and robustness of damage detection methods. For example, Mehrian et al. [22] integrated the flexibility matrix and modal data within a hybrid approach, which enabled the detection of multiple damages, although its accuracy decreased under noisy conditions. Vaez and Fallah [23] combined modal data with the GA–PSO algorithm for thin plates, achieving higher accuracy and faster convergence compared to single-indicator methods. Rokhsati et al. [24] proposed three novel objective functions based on Modal Strain Energy (MSE), the Generalized Flexibility Matrix (GFM), and mode shapes, demonstrating that the combination of MSE and mode shapes yielded the best performance. Similarly, Huang et al. [25] combined substructure decomposition, element-relative modal strain energy (ER-MSE), and an improved WOA with Lévy flights (LWOA), thereby enhancing accuracy in estimating damage severity. Nouri et al. [26] further showed that statistical pattern recognition techniques applied directly to vibration signals can effectively detect nonlinear damage. Sabzevari et al. [27] introduced a vibration-based damage identification framework for moment frames, in which modal parameters were incorporated into metaheuristic optimization algorithms to accurately locate and quantify structural damage. Among FEM model updating approaches, data-driven methods have attracted significant research interest through various applications such as time-series modeling [28], and application of deep ensemble learning for zero-shot damage detection [29]. These studies collectively indicate that multi-parameter objective functions, particularly those integrating several modal indicators, can overcome the shortcomings of single indicators and provide greater reliability under noisy or incomplete measurement conditions.

With the growing adoption of multi-parameter objective functions for improved damage detection, research efforts increasingly focused on the selection and application of optimization algorithms. In early studies, various standalone metaheuristic algorithms were widely employed and demonstrated notable performance under certain conditions. Nevertheless, they also exhibited common shortcomings, including premature convergence, sensitivity to noise, and high computational costs. Hosseinzadeh et al. [30], for example, proposed a baseline updating approach using modal residual force in combination with the Grey Wolf Optimizer, which enhanced both localization and severity detection. Such weaknesses motivated researchers to develop hybrid algorithms, aiming to combine the strengths of different strategies and achieve a better balance between exploration and exploitation, thereby improving accuracy and robustness. In this context, several notable contributions include the work of Chen and Yu [31], who introduced a PSO–Nelder–Mead hybrid method; Nguyen et al. [32], who integrated PSO with Artificial Neural Networks; and Chen et al. [33], who proposed the W-ChOA algorithm. Moreover, Zhang et al. [34] developed a hybrid optimization framework based on the combined correlation of acceleration and strain responses, which eliminated the need for predefined reference points and achieved high accuracy and robustness even under noisy conditions. A review of previous studies indicates that, despite extensive efforts, several critical challenges in structural damage detection remain unresolved. Objective functions based on single indicators have limited capability in accurately localizing damage and show degraded performance under noisy conditions. Although multi-parameter objective functions have improved accuracy, their effectiveness often depends on the specific optimization algorithm employed and still requires more comprehensive evaluation. On the other hand, standalone metaheuristic algorithms, while each possessing unique advantages, also suffer from weaknesses such as premature convergence, sensitivity to noise, and high computational costs. Hybrid algorithms have addressed some of these limitations; however, most of them are still relatively new, require further simplification and development, and in many cases lack comprehensive comparative assessments under identical conditions.

In response to these limitations, the present study introduces three main contributions. First, a novel objective function is proposed, designed by combining three key dynamic indicators—natural frequencies, mode shapes, and modal strain energy—which can be effectively employed alongside different metaheuristic algorithms. Second, a systematic comparison is conducted among several well-known metaheuristic algorithms, including GOA, WOA, MRFO, SBOA, and AOA, to evaluate their performance under different damage scenarios and noise levels. Third, a new hybrid algorithm (MSOA) is developed, which integrates the global exploration capability of MRFO with the local exploitation strength of SBOA through an adaptive switching mechanism, thereby enabling highly accurate and robust damage detection even under complex and noisy conditions.

2. Mathematical model of structural damage detection

2.1. Modal analysis

Modal analysis is a fundamental technique for characterizing the dynamic behavior of multi-degree-of-freedom (MDOF) systems. It provides essential modal parameters, including natural frequencies, mode shapes, and modal strain energy, which describe the vibrational characteristics of the structure and serve as the basis for damage detection. In this study, these parameters are computed by solving the eigenvalue problem of the structural system, with numerical implementation carried out in MATLAB.

The governing equation of motion for an undamped MDOF system is expressed as, (Eq. (1)) [35,36].

$$[M]\{\ddot{u}\} + [K]\{u\} = \{P\} \tag{1}$$

where $[M]$ is the mass matrix, $[K]$ is the stiffness matrix, and $\{u\}$ is the displacement vector. Considering free vibration and assuming a harmonic solution of the form $\{u\} = \emptyset e^{i\omega t}$, the equation can be reduced to the classical eigenvalue problem in Eq. (2).

$$[K - \omega_i^2 M]\emptyset_i = 0 \qquad i = 1, 2, \dots, n \tag{2}$$

where ω_i is the angular frequency, $\emptyset_i$ is the corresponding mode shape vector for the ith mode, and n denotes the number of degrees of freedom. Solving Eq. (2) yields the natural frequencies and their associated mode shapes.

The natural frequencies are arranged into a diagonal matrix in Eq. (3).

$$[\omega^2] = \begin{bmatrix} \omega_1^2 & \dots & 0 \\ \vdots & \ddots & \vdots \\ 0 & \dots & \omega_n^2 \end{bmatrix} \tag{3}$$

The mode shapes are obtained as eigenvectors corresponding to the eigenvalues of Eq. (2). These vectors are assembled into the modal matrix in Eq. (4).

$$[\emptyset] = \begin{bmatrix} \emptyset_{11} & \dots & \emptyset_{1n} \\ \vdots & \ddots & \vdots \\ \emptyset_{n1} & \dots & \emptyset_{nn} \end{bmatrix} \tag{4}$$

The modal strain energy (MSE) represents the elastic energy stored within the structure in a given mode. For the ith element in the jth mode, it can be written in Eq. (5).

$$U_i^j = \frac{1}{2}\emptyset_{i,j}^T K_i \emptyset_{ij} \tag{5}$$

K_i, is the stiffness matrix of the structure's ith element, and $\emptyset_{i,j}$ is the mode shape vector associated with element i in mode j. Collecting the strain energy values for all elements and modes yields the following matrix form in Eq. (6).

$$[MSE] = \begin{bmatrix} U_1^1 & \dots & U_1^j \\ \vdots & \ddots & \vdots \\ U_i^1 & \dots & U_i^j \end{bmatrix} \tag{6}$$

2.2. Definition of structural damage

In this study, the structural damage detection problem is formulated as an optimization task. Structural damage can be modeled in various ways, such as reductions in the stiffness, mass, or damping matrices. Stiffness reduction may, in turn, be represented through a decrease in the elastic modulus of structural elements or in their moment of inertia. Here, stiffness reduction is adopted as the primary modeling approach, since within the investigated damage range, variations in the mass matrix are negligible, and stiffness changes provide the most reliable indicator for identifying both the presence and severity of damage.

The damage index a_i is introduced for the ith element, ranging from 0 (undamaged) to 1 (fully damaged), to represent the percentage reduction in its stiffness. The stiffness of the damaged element is expressed in Eq. (7).

$$\mathrm{K}_i^a = \mathrm{K}_i(1 - a_i) \tag{7}$$

where K_i^a denotes the stiffness of the ith element in the damaged state, K_i is the stiffness of the undamaged element, and a_i is the damage index.

The global stiffness matrix of the damaged structure is then assembled by combining the stiffness contributions of all elements as a function of their respective damage indices in Eq. (8).

$$K(a_1, \dots, a_n) = \bigcup_1^n K_i^a \tag{8}$$

Here, $K(a_1, \dots, a_n)$ is the total stiffness matrix of the damaged structure and n is the number of elements in the finite element model.

2.3. Noise addition

Although model updating techniques that incorporate variations in structural flexibility can achieve high precision, their applicability is limited to cases where reliable flexibility data for the damaged structure are available. To assess the robustness of such methods against measurement inaccuracies, researchers commonly introduce several levels of random error.

In practice, however, external disturbances—such as environmental effects from ambient loading or uncertainties in sensor placement—may significantly affect the accuracy of recorded flexibility data, leading to higher levels of measurement error. In contrast, natural frequencies can generally be identified with high precision using modern accelerometers. As a result, some studies reconstruct structural stiffness properties primarily from accurately measured natural frequencies. Nevertheless, the corresponding sensitivity equations are still highly vulnerable to unanticipated inaccuracies in frequency data.

To simulate these effects, noise is incorporated into the frequency measurements of the damaged structure using the following expression in Eq. (9).

$$[\omega_n] = [\omega] \times (1 + N \times rand) \tag{9}$$

Where ω_n represents the noisy frequency vector, N denotes the noise level, and $rand$ is a uniformly distributed random number between 0 and 1.

2.4. Objective function formulation

The objective function, is formulated to quantify discrepancies between the dynamic characteristics of the undamaged and damaged states. It is defined as Eq. (10).

$$Objective\ function = |1 - (f_1 \times f_2 \times f_3)| \tag{10}$$

where f_1, f_2, and f_3 are three complementary terms based on natural frequencies, mode shapes, and modal strain energy, respectively. Minimization of the objective function yields the set of damage indices that best reproduce the dynamic behavior of the damaged structure.

The first component, f_1, evaluates the similarity of natural frequencies between the model and the damaged structure is obtained as Eq. (11).

$$f_1 = \frac{\sum_{i=1}^{n} b_i}{n} \quad , \quad b_i = \frac{\min(\omega_{n,d}^2, \omega_{n,m}^2)}{\max(\omega_{n,d}^2, \omega_{n,m}^2)} \tag{11}$$

where $[\omega_{n,d}]$ and $[\omega_{n,m}]$ are the ith natural frequencies of the damaged and model structures, respectively.

The second component, f_2, measures the correlation between mode shapes of the damaged and model structures using the Modal Assurance Criterion (MAC). Eq. (12) shows the mathematical description of the MAC.

$$MAC\ (X,Y) = \frac{\left|X^T.Y\right|^2}{(X^T.X)(Y^T.Y)} \tag{12}$$

where ***X*** and ***Y*** are arbitrary vectors based on the user's choice, and *T* represents the matrix's transpose.

In this study, MAC is calculated for mode shapes and modal strain energy. MAC is calculated for mode shapes which is called "M.MAC" in Eq. (13).

$$M.MAC\ (\emptyset_i^d, \emptyset_i^m) = \frac{\left|\emptyset_i^{dT}.\emptyset_i^m\right|^2}{(\emptyset_i^{dT}.\emptyset_i^d)(\emptyset_i^{mT}.\emptyset_i^m)} \tag{13}$$

where $\emptyset_i^d$ and $\emptyset_i^m$ are the ith mode shape vectors for the damaged and model structures, respectively. Therefore, f_2, is obtained as Eq. (14).

$$f_2 = \sum_{i=1}^{n} \frac{M.MAC_i}{n} \tag{14}$$

The third component, f_3, employs the modal strain energy (MSE) matrix defined in Eq. (6). Therefore, Eq. (15) shows the MAC definition for each column of MSE matrix which is called "S.MAC".

$$S.MAC\ \left(MSE_i^d, MSE_i^m\right) = \frac{\left|MSE_i^{dT}.MSE_i^m\right|^2}{(MSE_i^{dT}.MSE_i^d)(MSE_i^{mT}.MSE_i^m)} \quad , \quad i = 1, \dots, n \tag{15}$$

where MSE_i^d and MSE_i^m are the ith column of MSE matrix for the damaged and model structures, respectively. Therefore, f_3, is obtained as Eq. (16).

$$f_3 = \sum_{i=1}^{n} \frac{S.MAC_i}{n} \tag{16}$$

In the proposed damage identification framework, the objective function is formulated to simultaneously account for multiple structural features sensitive to damage. Specifically, it is defined as the product of three components: f_1, f_2, and f_3.

The first term, f_1, quantifies the discrepancy between the natural frequencies of the damaged structure and those of the reference model. As natural frequencies are highly responsive to changes in mass and stiffness distribution, they primarily capture stiffness alterations caused by damage, providing critical insight into global dynamic behavior changes.

The second term, f_2, reflects the discrepancy between the mode shapes of the damaged structure and the reference model. Mode shapes describe vibration-induced deformation patterns and are sensitive to both global and local changes in structural properties. By incorporating mode shape information, f_2 enhances the objective function's ability to detect and localize damage, especially when frequency variations alone are insufficient.

The third term, f_3, captures differences in modal strain energy (MSE) distribution between the damaged structure and the reference model. Since strain energy is directly related to the internal force distribution and local stiffness of each element, this term provides strong sensitivity to local stiffness reductions. Incorporating MSE in the objective function therefore improves the localization of damage, allowing the identification of specific elements where stiffness degradation has occurred.

All three components are normalized to lie within the range [0,1], ensuring comparable contributions and preventing dominance of any single parameter.

The multiplicative formulation is deliberately chosen to emphasize the joint consistency of the indicators. Unlike additive forms, where one strong feature may compensate for a weak one, the product enforces agreement across all three features. If any component indicates a significant discrepancy, the overall objective function value reflects this, thereby penalizing inconsistent solutions.

As a result, the proposed objective function simultaneously considers global frequency shifts, mode shape deviations, and localized strain energy variations. This integrated and penalizing formulation enhances robustness in noisy environments and ensures reliable damage identification with improved accuracy in both localization and quantification. The complete formulation is provided in Eq. (10). The proposed procedure is illustrated in Fig. 1.

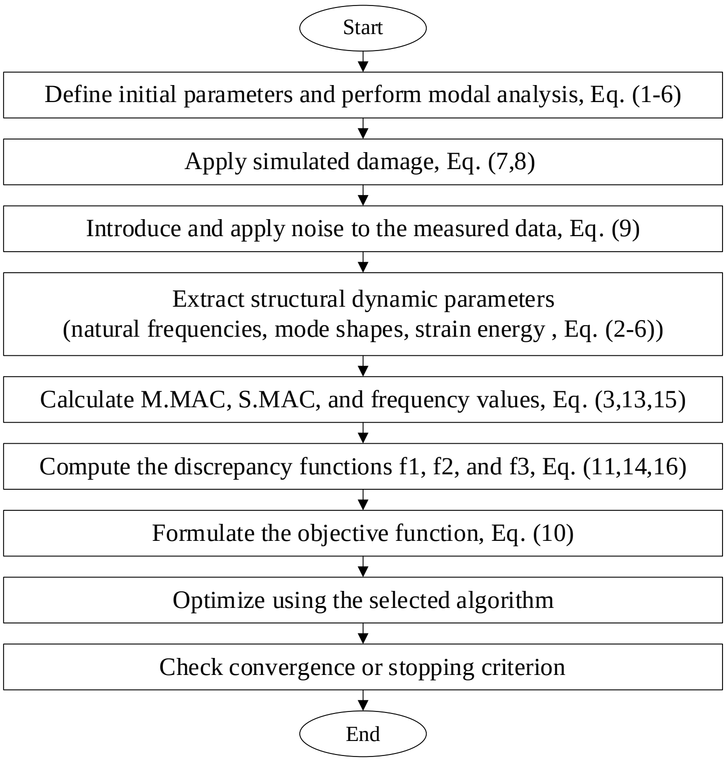

Fig. 1. Flowchart of damage detection method.

3. Optimization algorithms

This study employs five advanced metaheuristic optimization algorithms to address the structural damage identification problem in a two-dimensional moment-resisting frame. These algorithms are utilized to minimize the proposed objective function formulated from structural dynamic characteristics. Their selection is motivated by their demonstrated capability in solving complex, nonlinear, and high-dimensional optimization problems, as well as their adaptability to multi-objective scenarios. The algorithms considered in this research are:

1. Grasshopper Optimization Algorithm (GOA)
2. Whale Optimization Algorithm (WOA)
3. Manta Ray Foraging Optimization (MRFO)
4. Secretary Bird Optimization Algorithm (SBOA)
5. Addax Optimization Algorithm (AOA)

3.1. Grasshopper optimization algorithm (GOA)

The GOA, proposed by Saremi et al. in 2017 [8]. simulates the swarming behavior of grasshoppers, governed by gravitational forces, wind advection, and social interactions. This mechanism enables a smooth transition from exploration to exploitation during the optimization process.

The position update rule for each grasshopper is given by Eq. (17):

$$X_i = \sum_{j=1, j\neq i}^{N} s(d_{ij}) \, . \, \hat{d}_{ij} + G + W \tag{17}$$

x_i, is the new position of the i^{th} grasshopper, d_{ij}, is the distance between individuals, $\hat{d}_{ij}$, is the unit vector, $s(d)$, is the social interaction function, G, represents gravitational pull, and W is wind advection. The social interaction function $s(d)$ is defined as Eq. (18):

$$s(d) = fe^{-d/l} - e^{-d} \tag{18}$$

with parameters f and l controlling the interaction strength. To enhance convergence, a linearly decreasing control parameter c is introduced. (Eq. (19)).

$$X_i^{(t+1)} = c \, . \left(\sum_{j=1, j\neq i}^{N} s(d_{ij}) \, . \, \hat{d}_{ij} \right) + T_g \tag{19}$$

T_g is the current best solution and, c decreases from c_{max} to c_{min}.
The overall procedure of GOA is illustrated in the Fig. 2, from swarm initialization to position updates.

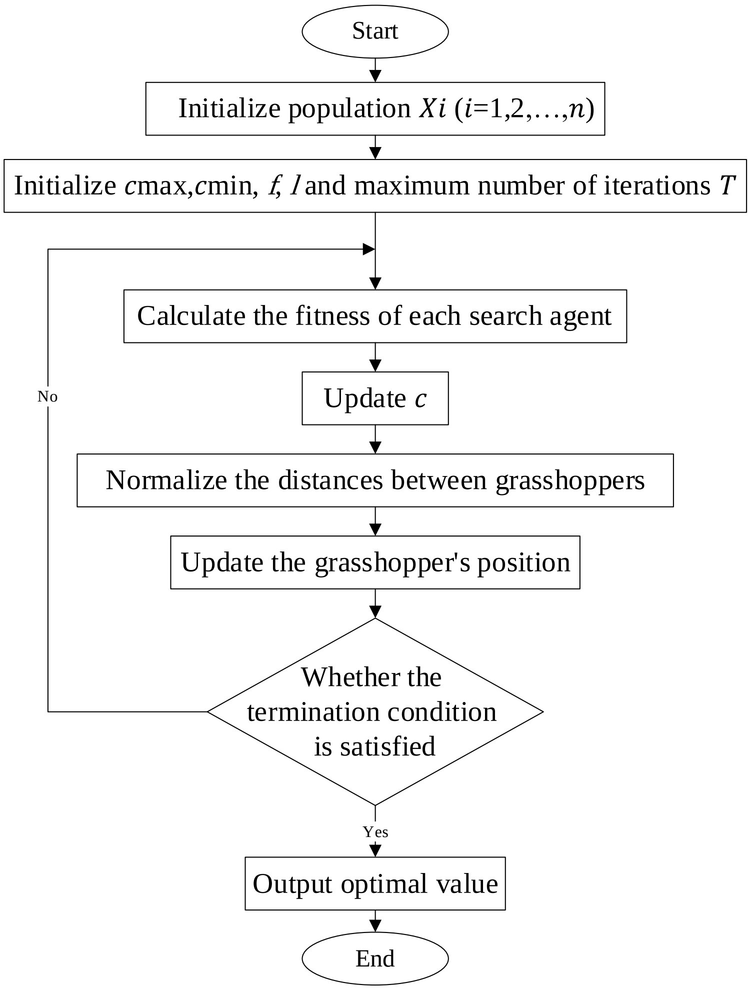

Fig. 2. Flowchart of the GOA.

3.2. Whale Optimization Algorithm (WOA)

The WOA, proposed by Mirjalili and Lewis in 2016 [6], is inspired by the bubble-net hunting strategy of humpback whales. In this mechanism, whales either encircle their prey, shrink the encircling path, or follow a spiral trajectory to simulate bubble-net attacks. These processes are mathematically modeled to guide the search agents toward optimal solutions. The flowchart of WOA is depicted in Fig. 3.

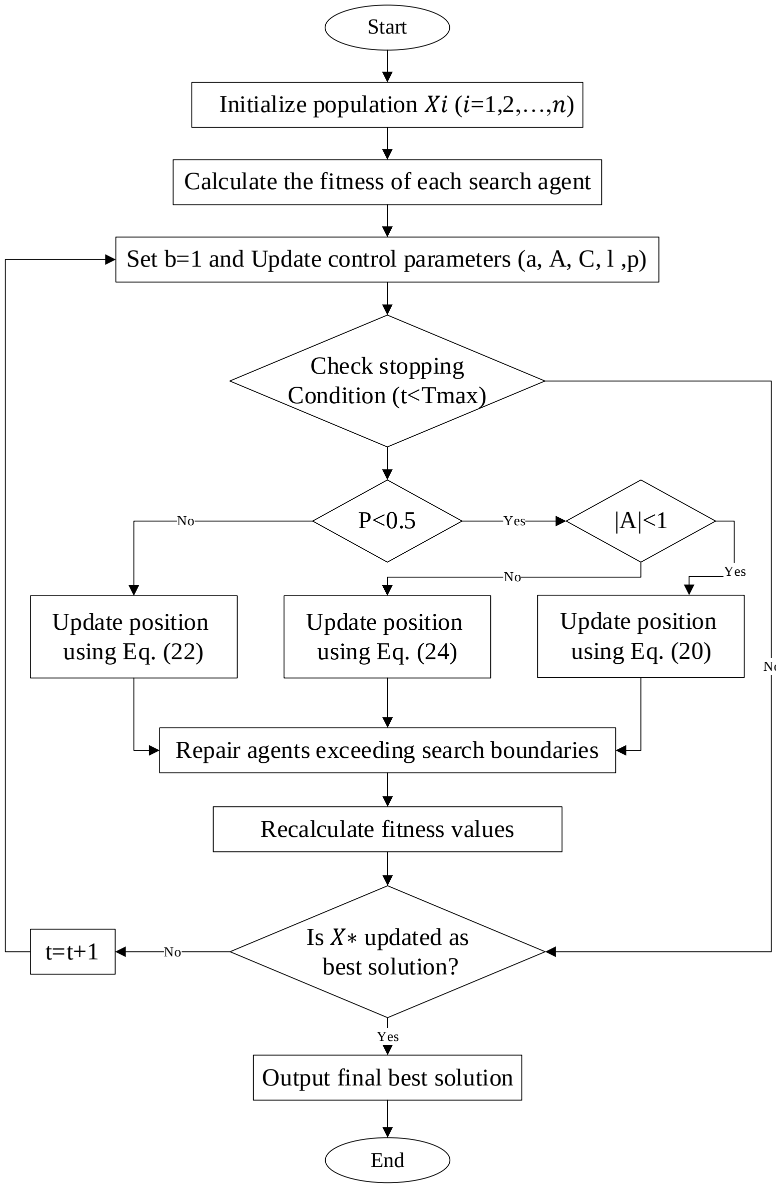

Fig. 3. Flowchart of the WOA.

3.2.1. Encircling prey

Whales first identify and encircle their prey, where the best-so-far solution ($\vec{X}^*(t)$) represents the prey. The distance and position update are defined as Eq. (20).

$$\vec{D} = \left|\vec{C}.\vec{X}^*(t) - \vec{X}(t)\right| \tag{20}$$

The updated position of each search agent is then computed according to Eq. (22).

$$\vec{X}(t+1) = \vec{X}^*(t) - \vec{A}.\vec{D} \tag{21}$$

t is the current iteration, $\vec{A} = 2\vec{a}.\vec{r} - \vec{a}$, $\vec{C} = 2.\vec{r}$, $\vec{a}$ decreases linearly from 2 to 0, and $\vec{r} \in [0,1]$ is a random vector.

3.2.2. Bubble-net attacking

Two strategies are employed: shrinking encircling and spiral updating. The spiral motion is modeled as Eq. (22).

$$\vec{X}(t+1) = \overrightarrow{D'}.e^{bl}.\cos(2\pi l) + \vec{X}^*(t) \tag{22}$$

Where $\overrightarrow{D'} = |\vec{X}^*(t) - \vec{X}(t)|$, b is a constant defining the logarithmic spiral shape, and $l \in [-1.1]$ is random. The choice between shrinking encircling and spiral updating is made with a 50% probability ($p \in [0.1]$) in Eq. (23).

$$\vec{X}(t+1) = \begin{cases} \vec{X}^*(t) - \vec{A}.\vec{D} & if\ p < 0.5 \\ \overrightarrow{D'}.e^{bl}.\cos(2\pi l) + \vec{X}^*(t) & if\ p \geq 0.5 \end{cases} \tag{23}$$

3.2.3. Search for prey

For exploration, $\vec{A}$ with $|\vec{A}| > 1$ is used to move search agents toward a random whale ($\vec{X}_{rand}$):

$$\vec{D} = |\vec{C}.\vec{X}_{rand} - \vec{X}|, \qquad \vec{X}(t+1) = \vec{X}_{rand} - \vec{A}.\vec{D} \tag{24}$$

3.3. Manta-Ray foraging optimization (MRFO)

The MRFO algorithm, introduced by Zhao et al. in 2020 [9], simulates the cooperative foraging strategies of manta rays, including chain foraging, cyclone foraging, and somersault foraging. These strategies allow MRFO to effectively switch between global exploration and local exploitation, leading to robust search performance. The overall procedure of MRFO is illustrated in Fig. 4.

The initialization step of the algorithm (Eq. (25)) involves randomly distributing candidate solutions within the design space based on the following expression.

$$X_i(t) = X_{min} + r * (X_{max} - X_{min}) \tag{25}$$

X_{min} and X_{max}, denote the bounds of the design variables, and $r \in [0,1]$ is a random number.

3.3.1. Foraging strategies

After initialization, the MRFO algorithm executes three distinct foraging strategies, inspired by the feeding behavior of manta rays, as detailed in the subsequent subsections.

3.3.1.1. Chain foraging

Each manta ray updates its position by following either the global best solution or its predecessor (Eq. (26)).

$$X_i^d(t+1) = \begin{cases} X_i^d(t) + r\left(X_{best}^d(t) - X_i^d(t)\right) + a\left(X_{best}^d(t) - X_i^d(t)\right) & for\ i = 1 \\ X_i^d(t) + r\left(X_{i-1}^d(t) - X_i^d(t)\right) + a\left(X_{best}^d(t) - X_i^d(t)\right) & for\ i = 2, \dots, N \end{cases} \tag{26}$$

Where $X_i^d(t)$ is current position of the i^{th} ray, X_{best} is current global best position, $r \in [0,1]$ is a random number controlling movement magnitude, N denote the population size and a indicates the weight factor, ($a = 2r\sqrt{|\log(r)|}$).

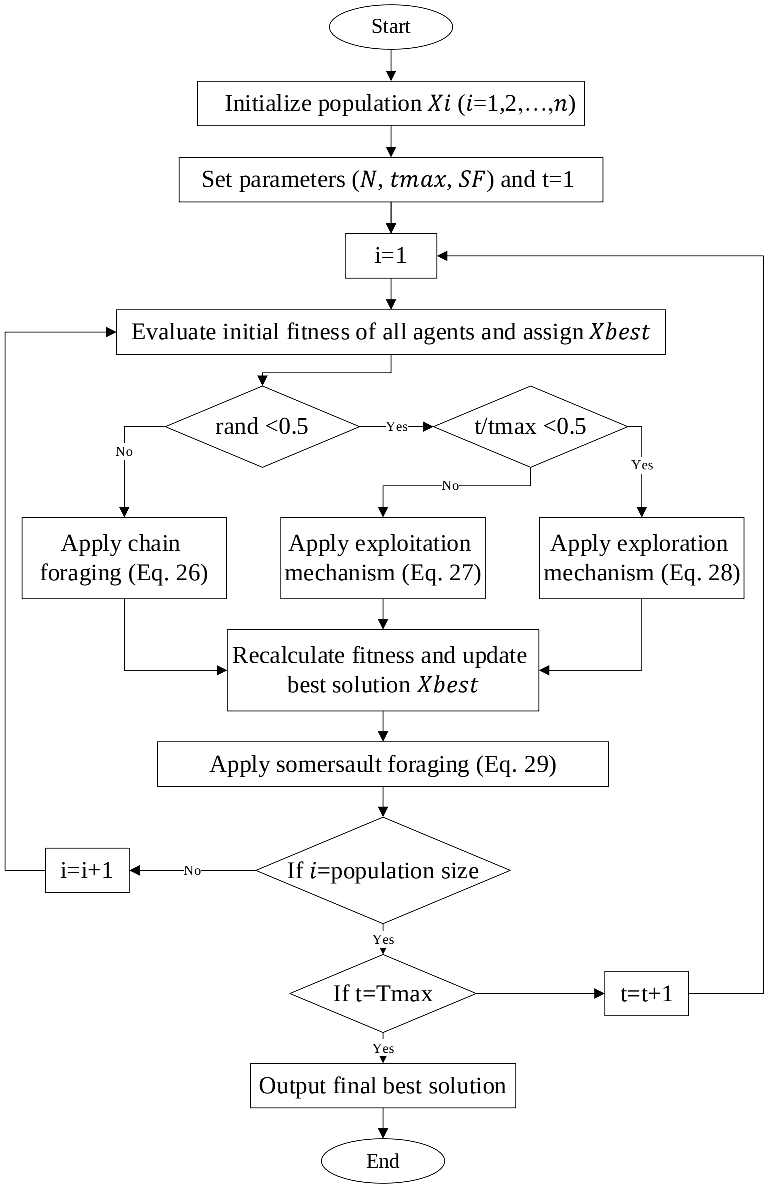

Fig. 4. Flowchart of the MRFO.

3.3.1.2. Cyclone foraging

This strategy simulates spiral swimming toward food, intensifying the search near the best candidate, (Eq. (27)).

$$X_i^d(t+1) = \begin{cases} X_{best}^d(t) + r\left(X_{best}^d(t) - X_i^d(t)\right) + \beta\left(X_{best}^d(t) - X_i^d(t)\right) & for\ i = 1 \\ X_{best}^d(t) + r\left(X_{i-1}^d(t) - X_i^d(t)\right) + \beta\left(X_{best}^d(t) - X_i^d(t)\right) & for\ i = 2, \dots, N \end{cases} \tag{27}$$

β is the weight factor, ($\beta = 2e^{r_1 \frac{t_{max}-t+1}{t_{max}}} * \sin(2\pi r_1)$). r_1 denotes a random value in the range [0, 1], and t_{max} indicates the maximum number of iterations.

Then, to enhance exploration capabilities, the algorithm randomly initializes individuals as Eq. (28).

$$X_i^d(t+1) = \begin{cases} X_{rand}^d(t) + r\left(X_{rand}^d(t) - X_i^d(t)\right) + a\left(X_{rand}^d(t) - X_i^d(t)\right) & for\ i = 1 \\ X_{rand}^d(t) + r\left(X_{i-1}^d(t) - X_i^d(t)\right) + a\left(X_{rand}^d(t) - X_i^d(t)\right) & for\ i = 2, \dots, N \end{cases} \tag{28}$$

$X_{rand}^d(t) = LL^d + r * (UL^d - LL^d)$, represents a randomly generated location within the search space. LL^d and UL^d denote the lower and upper bounds of dimension d, respectively.

3.3.1.3. Somersault foraging

This maneuver enables rays to periodically explore promising regions around the global best, (Eq. (29)).

$$X_i^d(t+1) = X_{rand}^d(t) + SF\left(r_2 X_{best}^d(t) - r_3 X_i^d(t)\right) \quad for\ i = 1, \dots, N \tag{29}$$

r_2 and r_3 are random numbers [0,1], SF refers to the somersault factor, ($SF = 2$).

3.4. Secretary bird optimization algorithm (SBOA)

The SBOA algorithm Introduced by Fu et al. in 2024 [10], is a population-based metaheuristic inspired by the unique hunting strategies of secretary birds. Each bird represents a candidate solution whose position is initialized as Eq. (30).

$$X_{i,j} = lb_j + r \times \left(ub_j - lb_j\right), i = 1, 2, \dots, N, j = 1, 2, \dots, Dim \tag{30}$$

X_i is denotes the position of the i-th secretary bird, lb_j and ub_j are the lower and upper bounds, respectively. The variable r is a random number ranging from 0 to 1.

The SBOA employs four phases inspired by secretary birds' behavior: hunting (exploration), consuming, attacking, and escaping (exploitation). This design allows the algorithm to alternate between global search and local refinement.

3.4.1. Hunting strategy

In the early phase ($t < \frac{1}{3}T$), differential evolution is used to simulate searching. The position of the secretary bird in this stage is updated using Eq. (31).

$$While\ t < \frac{1}{3}T, x_{i,j}^{new\ P1} = x_{i,j} + (x_{random_1} - x_{random_2}) \times R_1 \tag{31}$$

3.4.2. Consuming prey

When prey is found ($\frac{1}{3}T < t < \frac{2}{3}T$), Brownian motion drives position updates. This strategy is modeled in Eq. (32) and (33).

$$While\ \frac{1}{3}T < t < \frac{2}{3}T, x_{i,j}^{new\ P1} = x_{best} + \exp(\left(\frac{t}{T}\right)^4) \times (RB - 0.5) \times (\,x_{best} - x_{i,j}) \tag{32}$$

$$RB = rand(1, Dim) \tag{33}$$

3.4.3. Attacking prey

At later stages ($t > \frac{2}{3}T$), Levy flight enhances exploration. Position update during this phase is described by Eq. (34) and (35).

$$While\ t > \frac{2}{3}T, x_{i,j}^{new\ P1} = x_{best} + (\left(1 - \frac{t}{T}\right)^{\left(\frac{2t}{T}\right)} \times x_{i,j} \times RL \tag{34}$$

$$RL = 0.5 \times Levy(\mathrm{Dim}) \tag{35}$$

After generating a new candidate position in any of the three phases (hunting, consuming, or attacking), the solution is updated according to the following rule in Eq (36).

$$X_i = \begin{cases} x_i^{new,P1}, & if\ F_i^{new,P1} < F_i \\ X_i, & else \end{cases} \tag{36}$$

3.4.4. Escape strategy

The evasive behavior of secretary birds is modeled Eq. (37) and (38):

$$x_{i,j}^{new\ P2} = \begin{cases} C_1: x_{best} + (2 \times RB - 1) \times \left(1 - \frac{t}{T}\right)^2 \times x_{i,j}, if\ r\ and\ < r_i \\ C_2: x_{i,j} + R_2 \times \left(x_{random} - K \times x_{i,j}\right), else \end{cases} \tag{37}$$

$$X_i = \begin{cases} x_i^{new,P2}, & if\ F_i^{new,P2} < F_i \\ X_i, & else \end{cases} \tag{38}$$

The following flowchart in Fig.5 illustrates the steps involved in the SBOA.

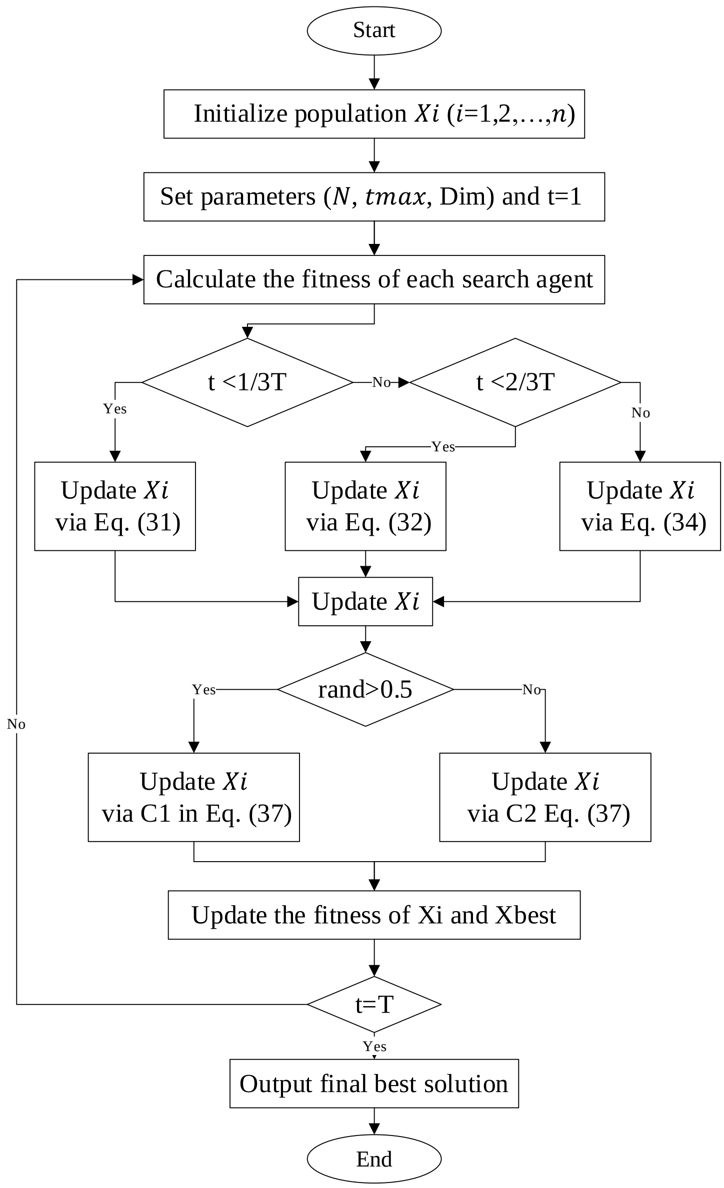

Fig. 5. Flowchart of the SBOA.

3.5. Addax optimization algorithm (AOA)

The AOA algorithm [11], is a population-based metaheuristic inspired by the survival strategies of addaxes in arid deserts. Each addax corresponds to a candidate solution in the search space. The initial position of the i-th addax in the d-th dimension is initialized as Eq. (39):

$$X_{i,d} = lb_d + r.(ub_d - lb_d) \tag{39}$$

lb_d and ub_d are the lower and upper bounds of the d-th dimension respectively, and r is a random number uniformly distributed in the interval [0,1].

AOA alternates between two phases that mimic the foraging and resting behaviors of addaxes, enabling both global exploration and local exploitation.

3.5.1. Foraging phase

In this phase, addaxes imitate their foraging behavior by tracking rainfall and moving toward vegetation-rich areas. Each agent selects a suitable foraging zone from candidates with better fitness (Eq. (40)) and updates its position as Eq. (41).

$$CA_i = \{X_k : F_k < F_i \ and \ k \neq i\} \tag{40}$$

$$x_{i,j}^{P1} = x_{i,j} + r_{i,j} \, . \left(SA_{i,j} - I_{i,j} . x_{i,j}\right) \tag{41}$$

The updated position replaces the old one if it improves the fitness in Eq. (42).

$$X_i = \begin{cases} x_i^{P1}, & F_i^{P1} \leq F_i \\ X_i, & else, \end{cases} \tag{42}$$

In this framework, SA_i refers to the selected foraging area for the ith addax, and $SA_{i,j}$ indicates the value of its jth dimension within that area. The term x_i^{P1} indicates the updated position of the ith agent during the foraging phase, with $x_{i,j}^{P1}$ specifying its jth dimension, and F_i^{P1} corresponds to the objective function value at this position. Additionally, $r_{i,j}$ represents uniformly distributed random numbers in the range [0,1], and $I_{i,j}$ denotes random integers selected from $\{1, 2\}$.

3.5.2. Digging phase

In the second phase, addaxes mimic the behavior of digging shallow pits for resting, leading to small local refinements (Eq. (43)).

$$x_{i,j}^{P2} = x_{i,j} + \left(1 - 2r_{i,j}\right) . \frac{ub_j - lb_j}{t} \tag{43}$$

t is the current iteration, and $r_{i,j}$ is uniformly random in [0,1] and the selection rule is applied as Eq. (44).

$$X_i = \begin{cases} x_i^{P2}, & F_i^{P2} \leq F_i \\ X_i, & else, \end{cases} \tag{44}$$

x_i^{P2} denotes the updated position of the ith agent in the digging stage, with $x_{i,j}^{P2}$ its jth dimension and F_i^{P2} the corresponding objective function value. The foraging (global exploration) and digging (local exploitation) steps are repeated until convergence or the maximum iteration limit, as illustrated in the AOA flowchart in Fig. 6.

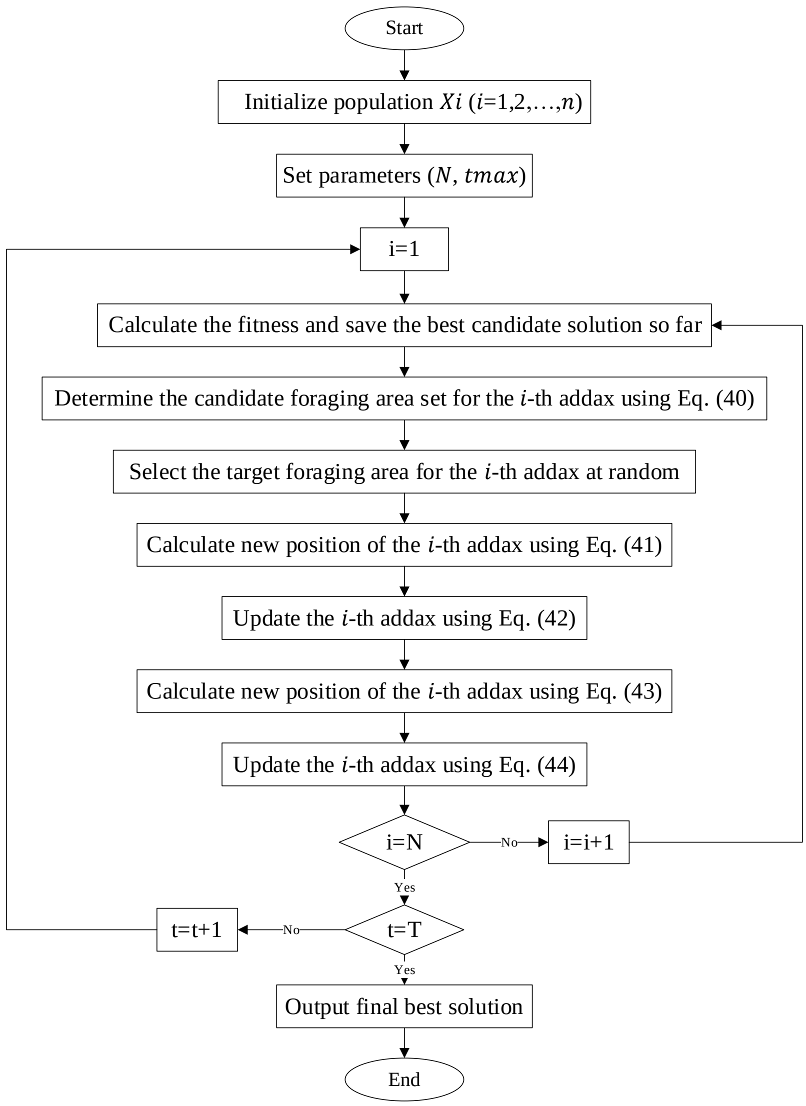

Fig. 6. Flowchart of the AOA.

In this study, five metaheuristic optimization algorithms—GOA, WOA, MRFO, SBOA, and AOA—were utilized, each inspired by distinct natural behaviors and designed with unique mechanisms for balancing exploration and exploitation. Their integration into the proposed framework allows for the accurate and robust solution of the inverse problem of structural damage identification. By leveraging the individual strengths of these algorithms, the method demonstrates reliable estimation of both damage location and severity, even under nonlinear, high-dimensional, and uncertain conditions. Moreover, the comparative assessment across different damage scenarios provides a comprehensive evaluation of their relative performance, thereby improving the robustness and reliability of the proposed damage detection framework.

4. Numerical modeling

To validate the effectiveness of the proposed methodology, numerical simulations are performed on a two-dimensional steel moment-resisting frame under different damage scenarios. The evaluation focuses on the performance of the proposed objective function and the accuracy of the employed optimization algorithms. For this purpose, only the first three vibration modes are considered, while the effect of measurement noise and various damage configurations are also included in the analysis. All simulations and computations are carried out in the MATLAB environment.

4.1. 19-Element moment frame

The case study structure is a two-dimensional moment-resisting frame consisting of 19 elements and 17 nodes, with each node having three degrees of freedom, as illustrated in Fig. 7. The material and geometric properties of the frame are summarized in Table 1, while the predefined damage scenarios are presented in Table 2.

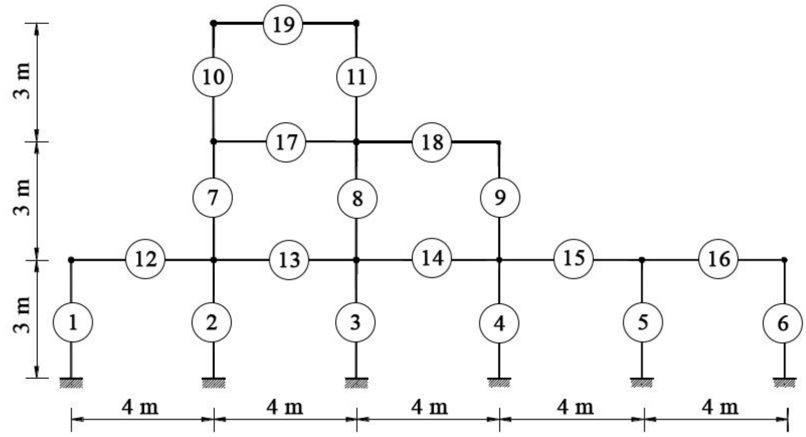

Fig. 7. Two-dimensional 19-element moment-resisting frame model.

Table 1
Cross-Sectional Properties.

Member Type	Area (m²)	Moment of Inertia ($\times10^{-4}$ m⁴)	Unit Weight (kg/m)	Elastic Modulus (GPa)
Beam (30×60 cm)	0.18	54	440.64	28.2
Column (40×40 cm)	0.16	21.3	391.68	28.2

Table 2
Damage Scenarios.

Scenario	Damaged Element	Damage Severity (%)
1	Element 2	10
	Element 18	15
2	Element 3	20
	Element 8	30
	Element 17	25

5. Damage identification results in 19-Element frame

To evaluate the performance of the five metaheuristic algorithms—GOA, WOA, MRFO, SBOA, and AOA—as well as the effectiveness of the proposed objective function, two predefined damage scenarios were analyzed under measurement noise levels of 0%, 3%, and 10%. For all algorithms, the maximum number of iterations was set to 2000, while the population sizes were 40 for GOA, 50 for WOA, 60 for MRFO, 40 for SBOA, and 30 for AOA. The accuracy of damage identification and the convergence trends of the objective function were then examined across all cases.

Fig. 8 and 9 show the damage identification results obtained using the GOA for Damage Scenarios 1 and 2 at different noise levels. Fig. 10 illustrates the convergence behavior of the objective function for both scenarios under the same noise conditions.

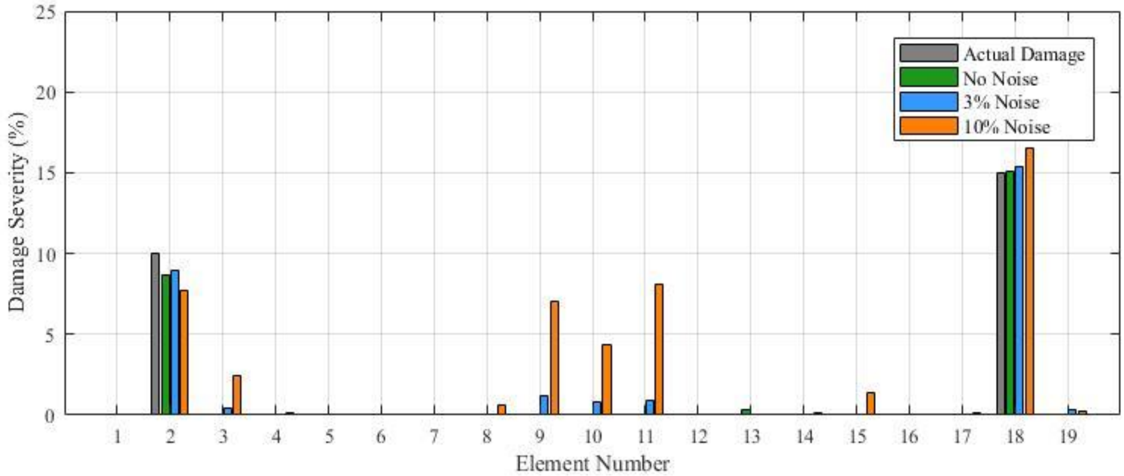

Fig. 8. Identified damage severities for Damage Scenarios 1 under varying noise levels - GOA.

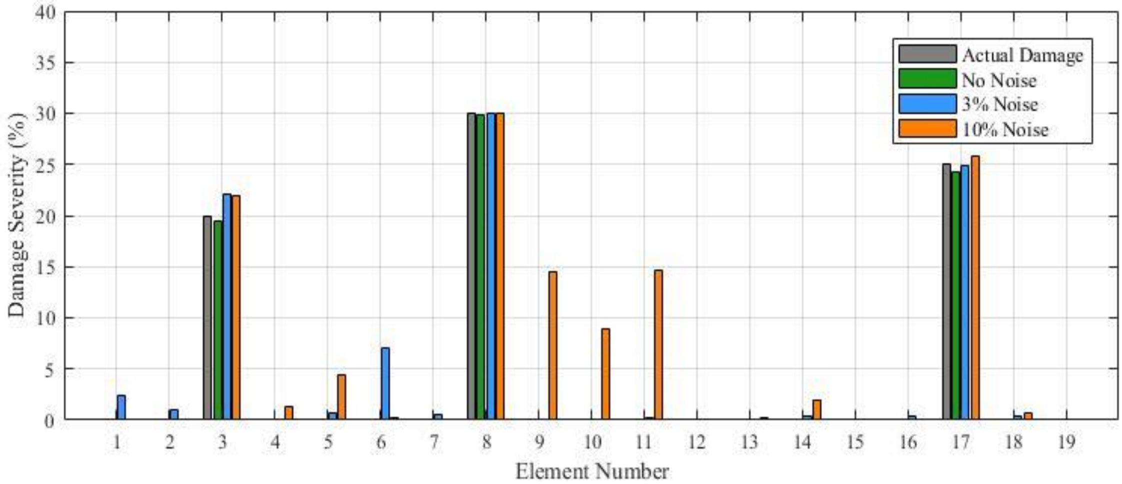

Fig. 9. Identified damage severities for Damage Scenarios 2 under varying noise levels - GOA.

The GOA demonstrated high accuracy in identifying damage in the absence of noise for both scenarios. Although the estimated severities were slightly lower than the actual values, no false positives were observed in undamaged members. In Damage Scenario 1 with 3% noise, the damaged locations and severities were successfully captured, with only minor deviations. However, approximately five undamaged members were incorrectly flagged as damaged, though with very small severities. At 10% noise, the algorithm still detected the main damaged elements but introduced false damage reports in several undamaged members, in some cases with relatively large severities, which reduced the overall reliability.

In Damage Scenario 2 under 3% noise, the GOA correctly identified all damaged members, yet misclassified several undamaged ones, with two false severities reaching 2.4% and 7%. When the noise level increased to 10%, the algorithm's performance further deteriorated, producing false damage estimates of up to 14.6%, thereby highlighting the challenges of maintaining accuracy under high-noise conditions.

The convergence plots of GOA demonstrate effective reduction of the objective function under all noise levels (0%, 3%, and 10%) for both scenarios. In noise-free conditions, the objective function decreased smoothly, reaching values close to zero at approximately 800 iterations. With 3% noise, convergence remained stable but slower, characterized by a shallower slope and requiring more iterations to approach near-zero values. Under 10% noise, Scenario 1 exhibited a convergence trend similar to that under 3% noise, whereas Scenario 2 showed noticeable oscillations. These results indicate that although GOA maintains strong convergence speed and stability, its accuracy is considerably affected in high-noise conditions.

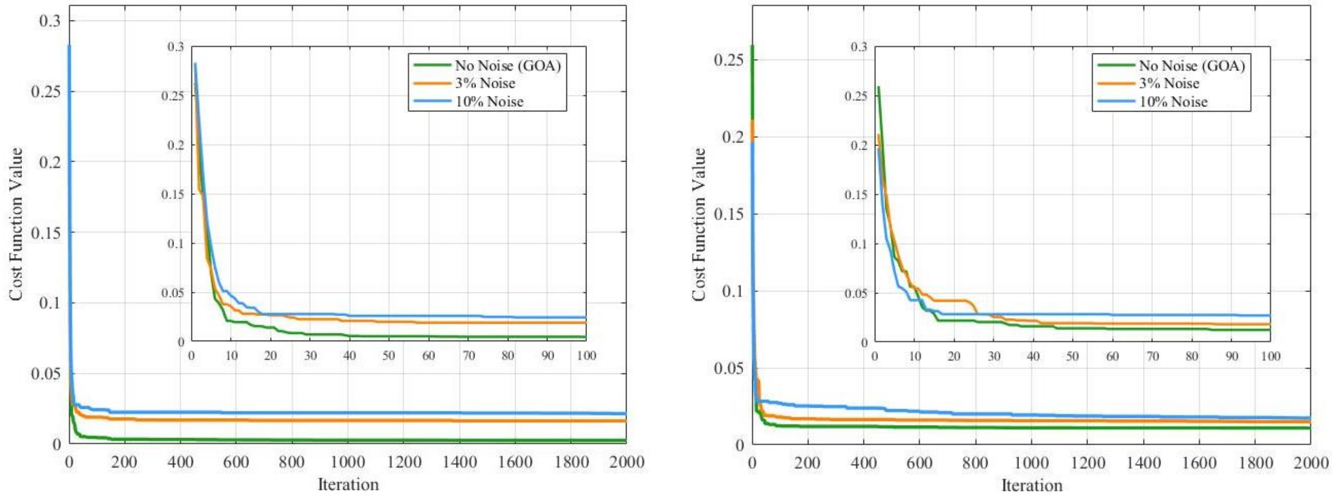

Scenario 1 Scenario 2

Fig. 10. Objective function convergence for Damage Scenario 1 and 2 under varying noise levels - GOA.

Fig. 11 and 12 present the damage identification results obtained using the WOA for Damage Scenarios 1 and 2 at noise levels of 0%, 3%, and 10%. Fig. 13 illustrates the corresponding convergence curves of the objective function for both scenarios under these noise conditions.

Under noise-free conditions, WOA successfully identified the damaged elements in both scenarios. Although the estimated severities slightly deviated from the actual values, only a few undamaged members were falsely classified, with negligible severities. In Damage Scenario 1 with 3% noise, WOA tended to slightly overestimate the severities and incorrectly flagged several undamaged members, with false severities up to 2.7%. At 10% noise, the algorithm still captured the primary damaged elements but introduced false reports in multiple undamaged members, with severities reaching 7.2%, thereby reducing the reliability of the results.

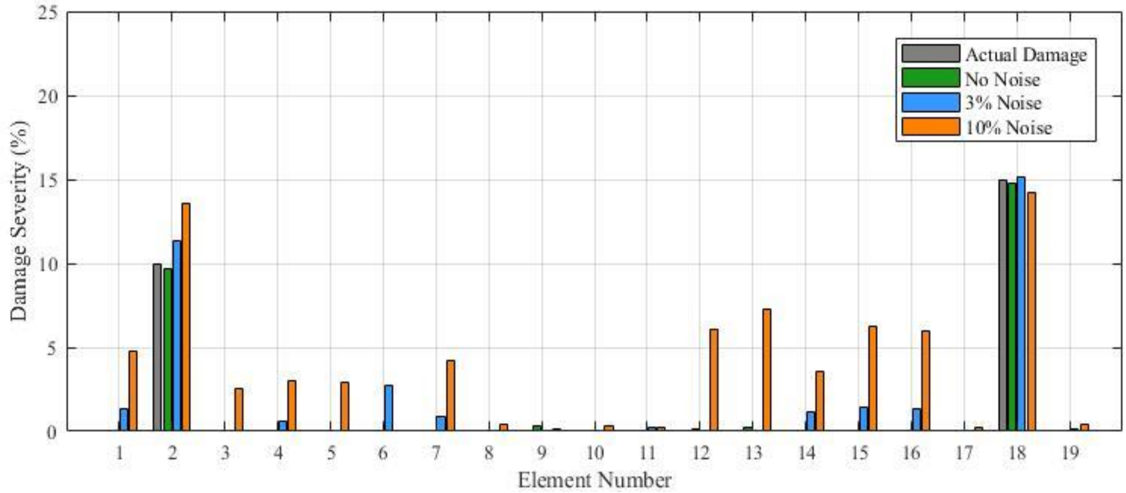

Fig. 11. Identified damage severities for Damage Scenarios 1 under varying noise levels - WOA.

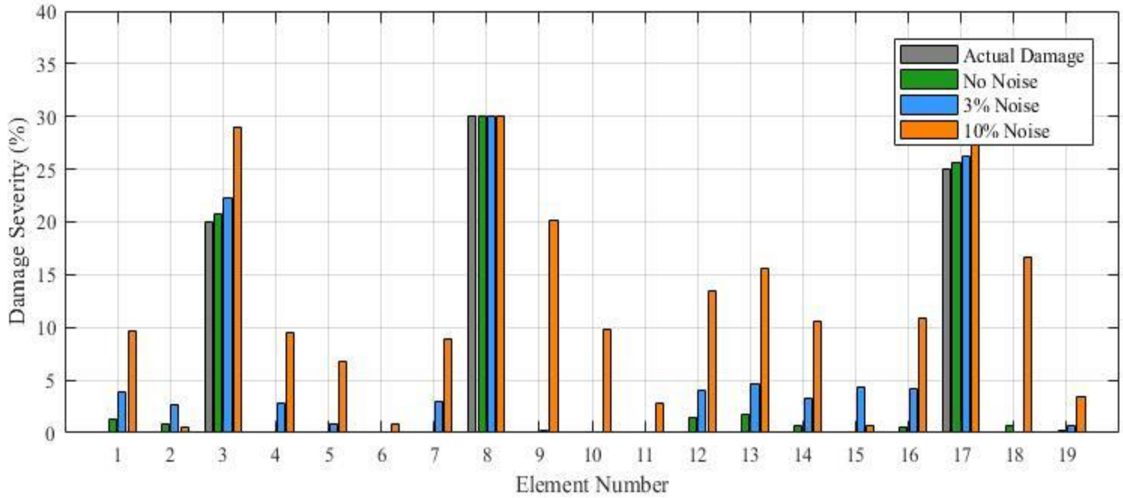

Fig. 12. Identified damage severities for Damage Scenarios 2 under varying noise levels - WOA.

In Damage Scenario 2 under 3% noise, WOA accurately located the damaged member and its severity but misclassified several undamaged ones, with false severities of 2.4% and 7%. When the noise level increased to 10%, the performance degraded further, with false damage reports reaching 20.1%, rendering the results unreliable in high-noise conditions.

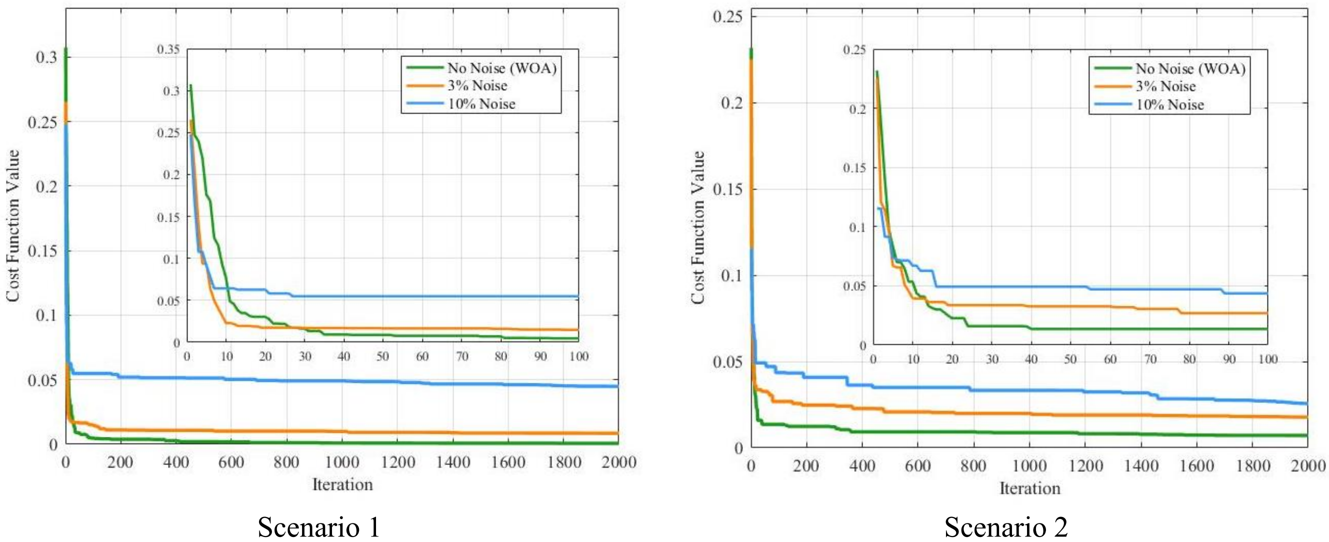

Fig. 13. Objective function convergence for Damage Scenario 1 and 2 under varying noise levels - WOA.

The convergence behavior of WOA demonstrates effective reduction of the objective function across all noise levels. In noise-free cases, the function decreased rapidly with minor oscillations, converging smoothly to near-zero values around 1800 iterations. With 3% noise, convergence remained stable but slower, showing a shallower slope and reduced precision. At 10% noise, a similar trend was observed, though the final objective function value remained higher, indicating that WOA requires more iterations and its accuracy is considerably affected under high-noise conditions.

Fig. 14 and 15 present the damage identification results obtained using the MRFO algorithm for Damage Scenarios 1 and 2 at noise levels of 0%, 3%, and 10%. Fig. 16 illustrates the convergence behavior of the objective function for both scenarios across these noise conditions.

Under noise-free conditions, MRFO demonstrated outstanding accuracy in identifying both the locations and severities of damage in the two scenarios, with no false classification of undamaged members. In Damage Scenario 1 with 3% noise, the algorithm maintained strong performance, correctly detecting all damaged elements and their severities without misclassification. At 10% noise, MRFO continued to identify damage locations accurately and provided reasonably precise severity estimates, though a few undamaged members were falsely reported as damaged, with maximum false severities of 3.5%.

In Damage Scenario 2 under 3% noise, MRFO misclassified several undamaged members, but their reported severities were relatively small. At 10% noise, the algorithm still detected the true damaged elements and severities but produced false reports in several undamaged members, with severities up to 8.9%. Overall, MRFO proved to be highly reliable, particularly under moderate noise levels.

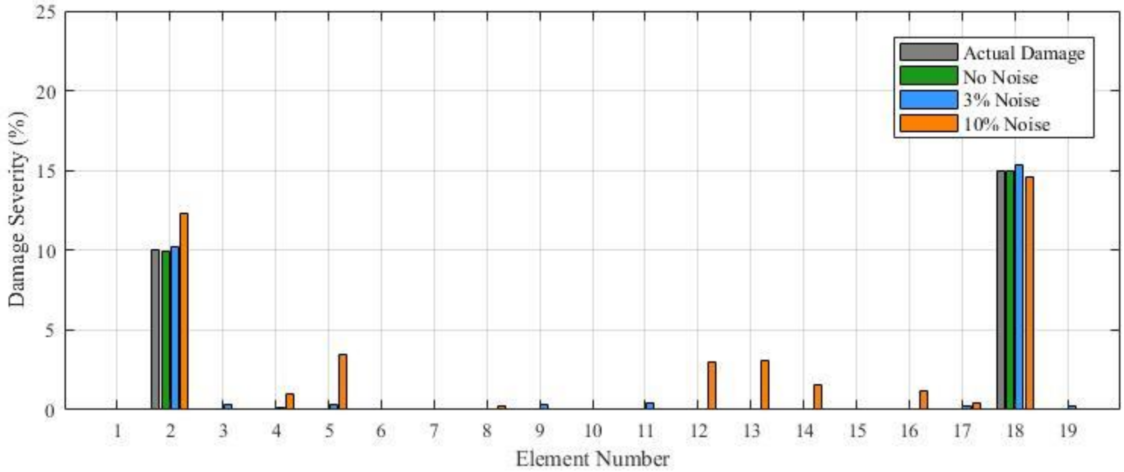

Fig. 14. Identified damage severities for Damage Scenarios 1 under varying noise levels - MRFO.

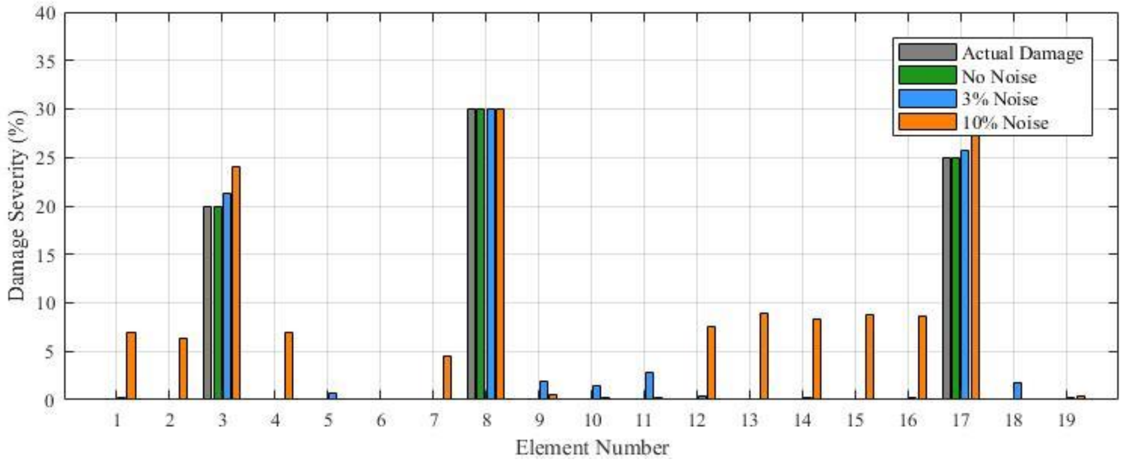

Fig. 15. Identified damage severities for Damage Scenarios 2 under varying noise levels - MRFO.

The convergence behavior of MRFO confirms its strong capability in minimizing the objective function across both scenarios and noise conditions. In noise-free cases, the objective function decreased sharply at the beginning, followed by mild fluctuations, and smoothly converged to near-zero around 1200 iterations. With 3% noise, convergence remained stable but slower, yielding slightly higher final values. At 10% noise, the same trend was observed, although the final values remained noticeably above zero. These results highlight MRFO's excellent accuracy under noise-free conditions, while also indicating that higher noise levels can reduce its detection precision.

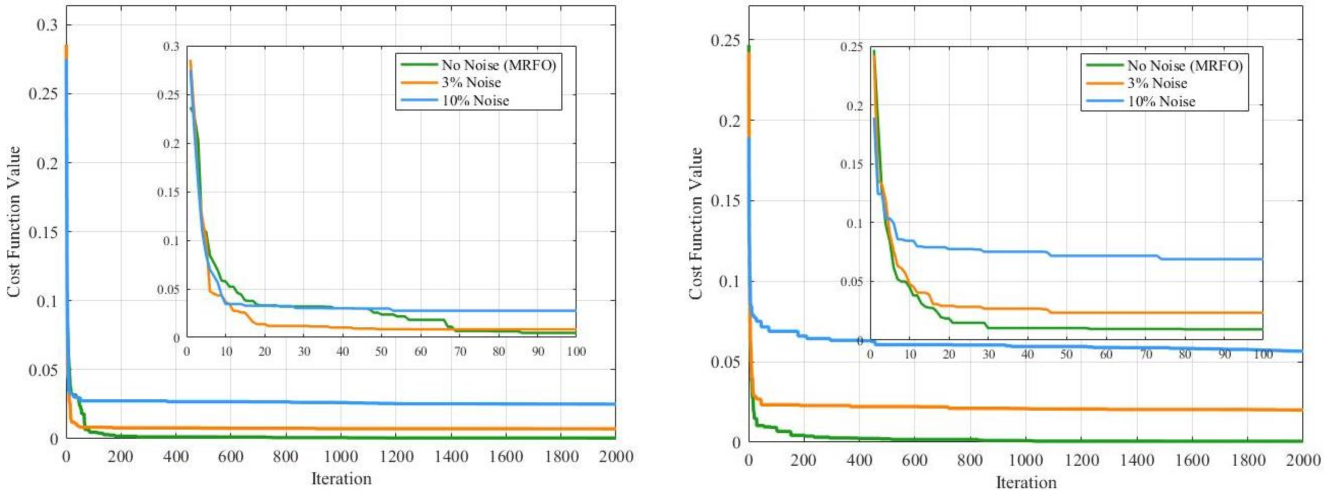

Scenario 1 Scenario 2

Fig. 16. Objective function convergence for Damage Scenario 1 and 2 under varying noise levels - MRFO.

Fig. 17 and 18 present the damage identification results obtained using the Satin Bowerbird Optimization Algorithm (SBOA) for Damage Scenarios 1 and 2 at noise levels of 0%, 3%, and 10%. Fig. 19 illustrates the convergence curves of the objective function for both scenarios under these noise conditions.

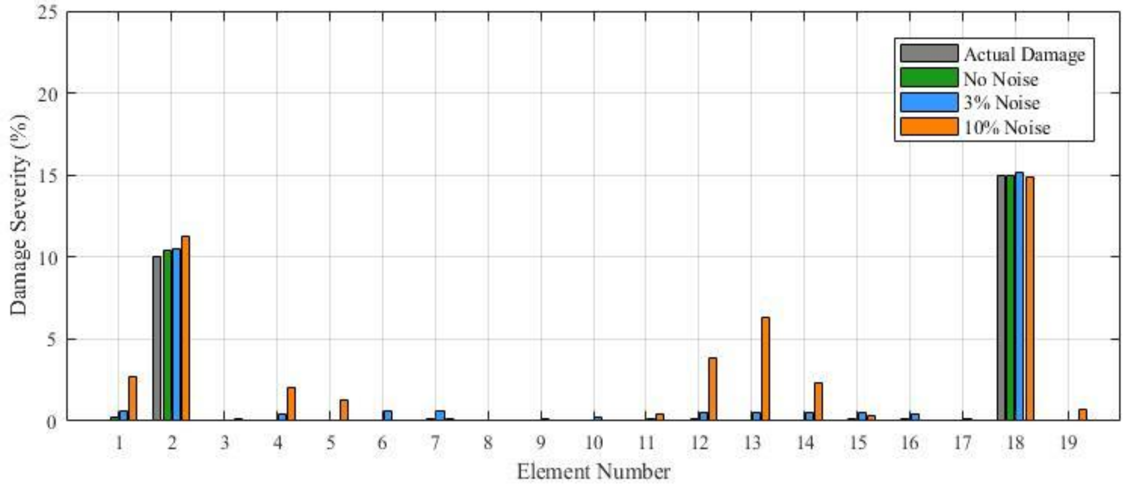

Fig. 17. Identified damage severities for Damage Scenarios 1 under varying noise levels - SBOA.

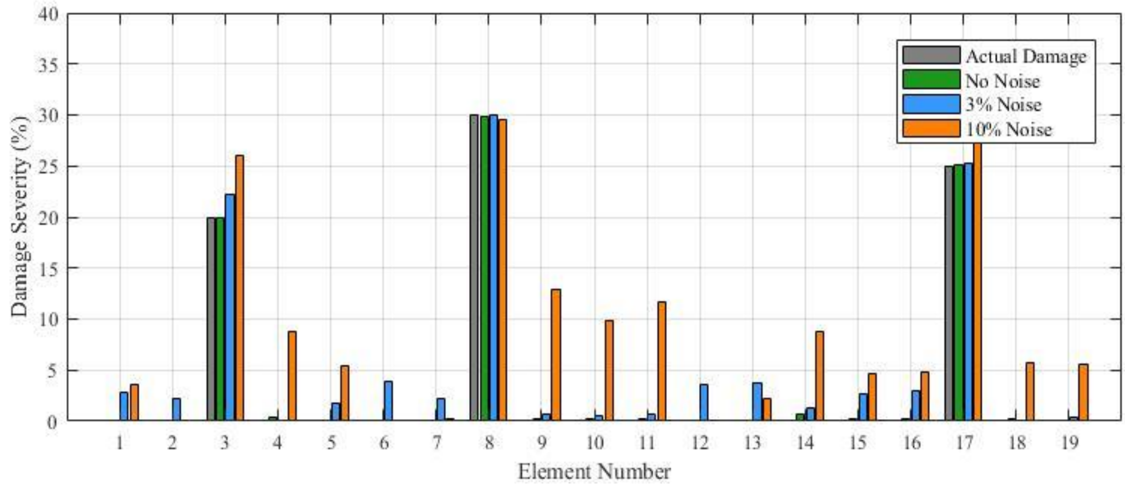

Fig. 18. Identified damage severities for Damage Scenarios 2 under varying noise levels - SBOA.

In the absence of noise, SBOA achieved high accuracy in identifying both the locations and severities of damage in both scenarios, with estimated severities closely matching the actual values. Although a few undamaged members were misclassified as damaged, the reported severities were negligible. In Damage Scenario 1 with 3% noise, SBOA maintained strong performance, accurately detecting all damaged locations and severities, while false positives were minimal. At 10% noise, the main damaged elements were still correctly identified and severity estimates remained reasonably accurate, though some undamaged members were falsely flagged, with severities up to 7.4%.

In Damage Scenario 2 with 3% noise, SBOA correctly identified the damaged element and its severity, while misclassified undamaged members showed only low severities, up to 3.9%. At 10% noise, the algorithm's performance declined, producing additional false positives with severities reaching 12.8%.

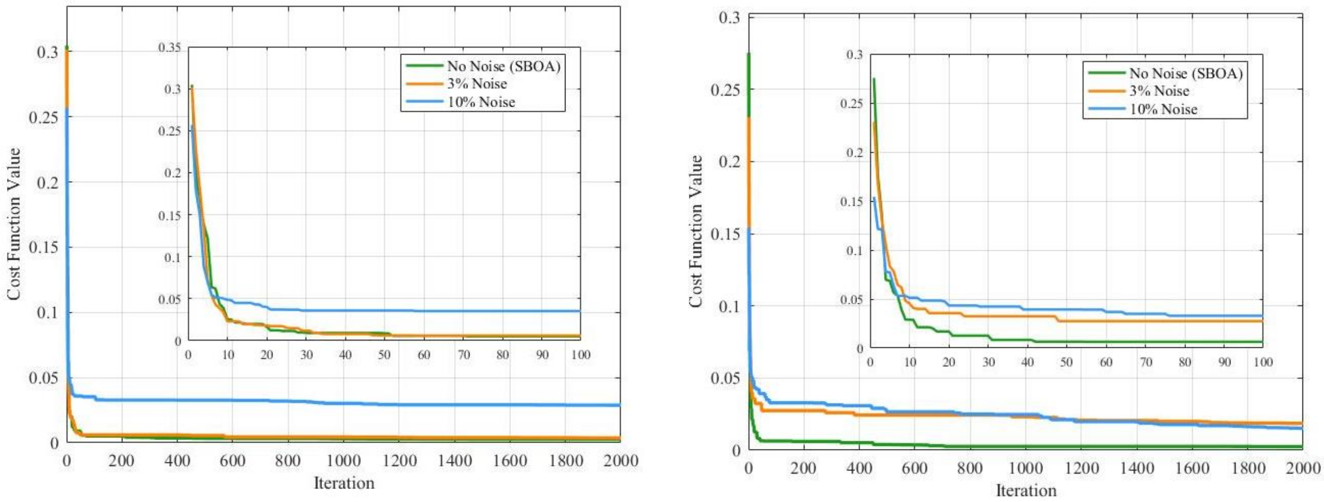

Scenario 1 Scenario 2

Fig. 19. Objective function convergence for Damage Scenario 1 and 2 under varying noise levels - SBOA.

The convergence curves of SBOA confirm effective minimization of the objective function across all scenarios and noise levels. In the noise-free case, the algorithm converged rapidly with slight initial oscillations, reaching near-zero values between 800 and 1000 iterations. With 3% noise, convergence remained stable and consistent, while at 10% noise the final objective function values were higher, though the algorithm still followed a clear downward trend. These results underline SBOA's strong convergence characteristics under low-noise conditions, with moderate reduction in precision at higher noise levels.

In Fig. 20 and 21, under noise-free conditions, AOA demonstrated high accuracy in identifying both damage locations and severities across the two scenarios, with only minimal deviations from the actual values. A few undamaged members were incorrectly flagged, with false severities not exceeding 1.5%. In Damage Scenario 1 with 3% noise, AOA accurately detected the damaged elements, although some undamaged members were misclassified with severities up to 2.8%. At 10% noise, the algorithm still located the true damaged components but produced false reports in several undamaged members, with severities reaching 7.8%.

In Damage Scenario 2 under 3% noise, AOA correctly identified the damaged element and its severity but misclassified multiple undamaged elements, with a maximum false severity of 8.8%. At 10% noise, its performance declined further, producing false severities as high as 16.8%, which reduced the overall reliability.

Figure 22 illustrates the convergence behavior of AOA.

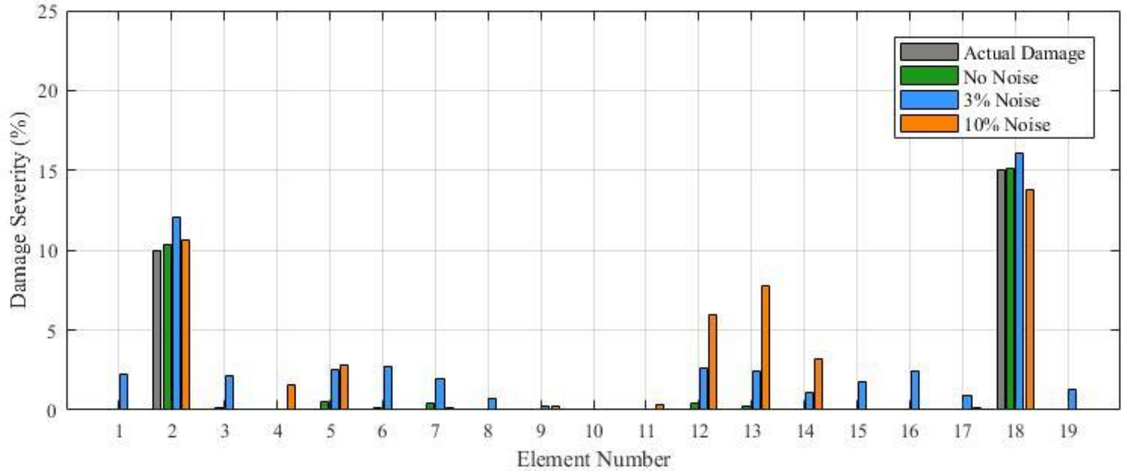

Fig. 20. Identified damage severities for Damage Scenarios 1 under varying noise levels - AOA.

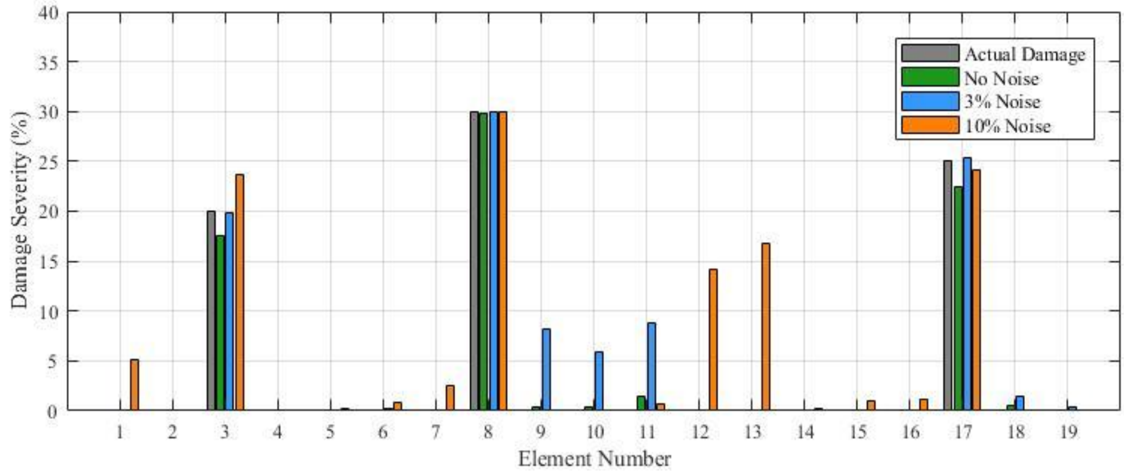

Fig. 21. Identified damage severities for Damage Scenarios 2 under varying noise levels - AOA.

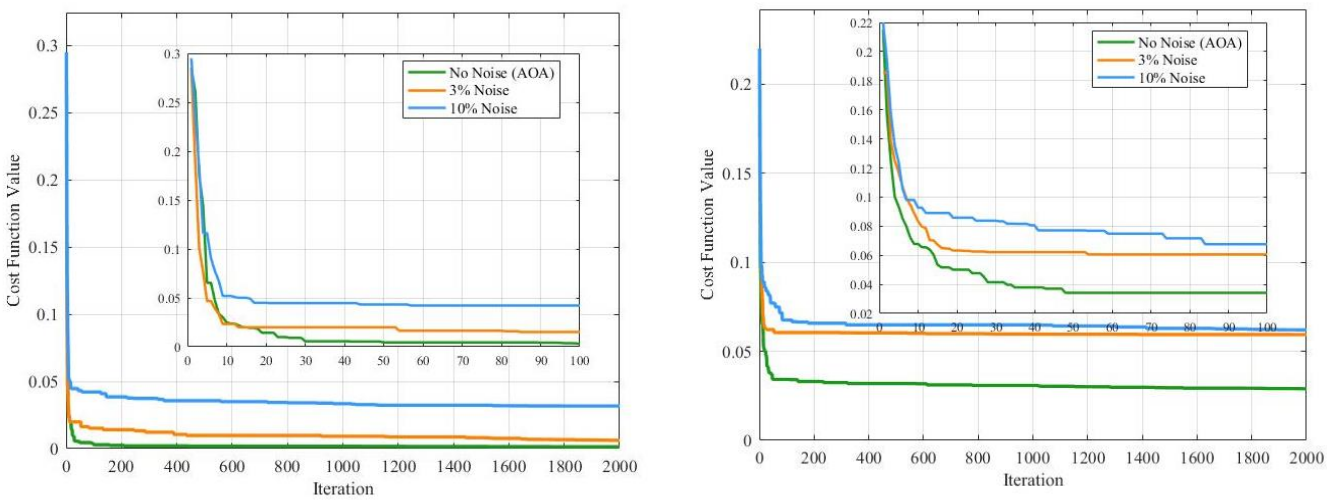

Scenario 1 Scenario 2

Fig. 22. Objective function convergence for Damage Scenario 1 and 2 under varying noise levels - AOA.

As shown in Fig. 22, the convergence behavior of AOA, highlights its ability to minimize the objective function across all noise levels and scenarios. AOA converged rapidly in all cases; however, it often stabilized at higher objective function values without reaching near-zero. Although convergence paths were generally smooth and consistent, increasing noise resulted in progressively higher final values. These results indicate that while AOA exhibits fast convergence, its tendency toward premature stabilization limits its accuracy under high-noise conditions.

Fig. 23 and 24 present the damage identification results of all optimization algorithms under noise-free conditions for Damage Scenarios 1 and 2. Across both cases, the proposed objective function achieved high accuracy with all algorithms. Among them, MRFO delivered the most precise results, whereas GOA showed the weakest performance in Scenario 1 and AOA in Scenario 2.

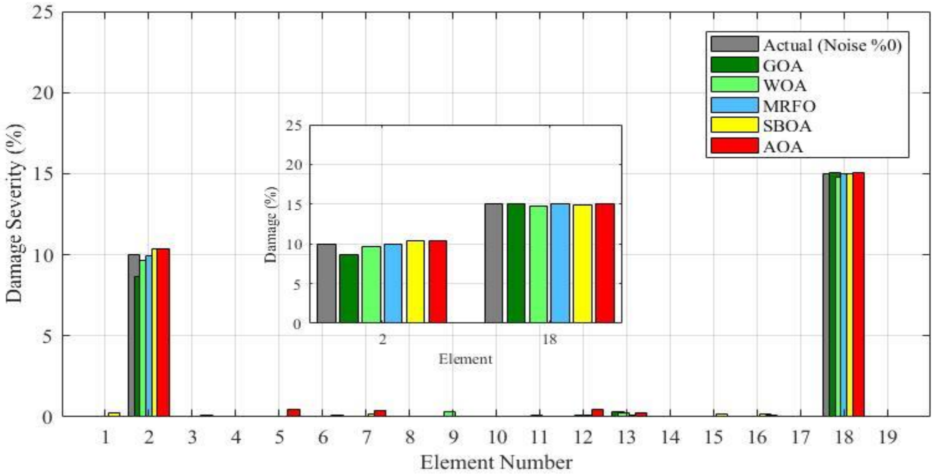

Fig. 23. Damage Identification Results – Scenario 1, Noise-Free (All Algorithms).

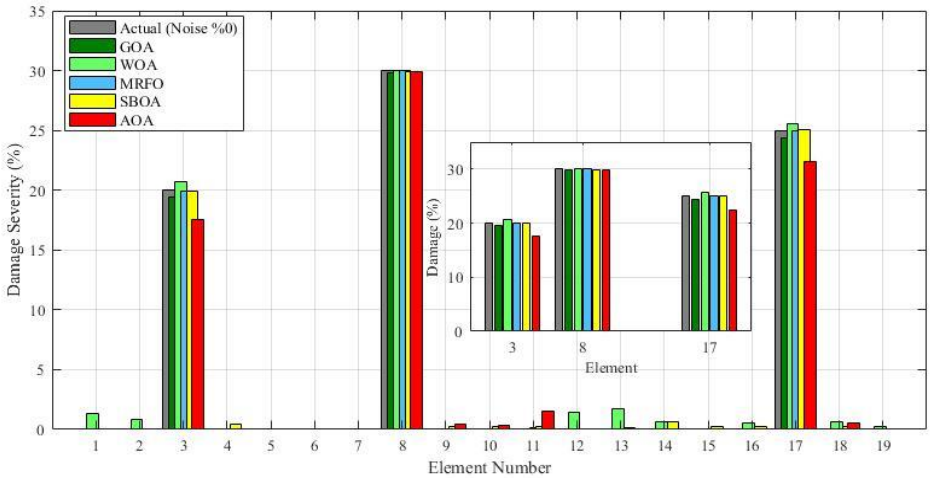

Fig. 24. Damage Identification Results – Scenario 2, Noise-Free (All Algorithms).

Fig. 25 and 26 illustrate the results under 3% noise. The objective function maintained reliable performance, with all algorithms correctly detecting damage locations and severities. Minor false positives were observed, as some undamaged elements were incorrectly flagged, though with low severities. MRFO exhibited the strongest noise robustness, while GOA remained effective despite slightly underestimating severities. By contrast, AOA showed reduced reliability due to an increased number of false positives.

Fig. 27 and 28 depict the outcomes under 10% noise. In these cases, higher noise levels increased false detections, although all algorithms still partially identified damage locations and severities. MRFO and

SBOA demonstrated the best noise resistance, sustaining higher accuracy, while GOA showed a notable decline by misclassifying several undamaged members as severely damaged. AOA and WOA performed least effectively, particularly in Scenario 2 with multiple damaged elements, where distinguishing between damaged and undamaged members proved more difficult.

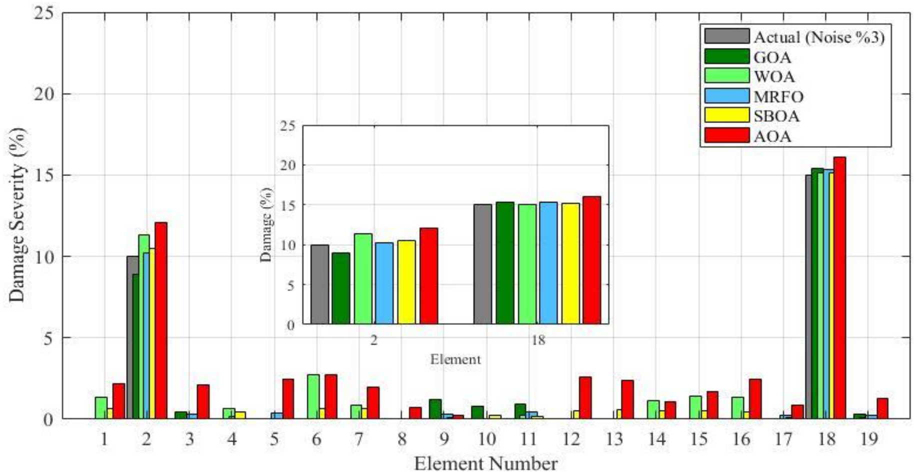

Fig. 25. Damage Identification Results – Scenario 1, 3% Noise (All Algorithms).

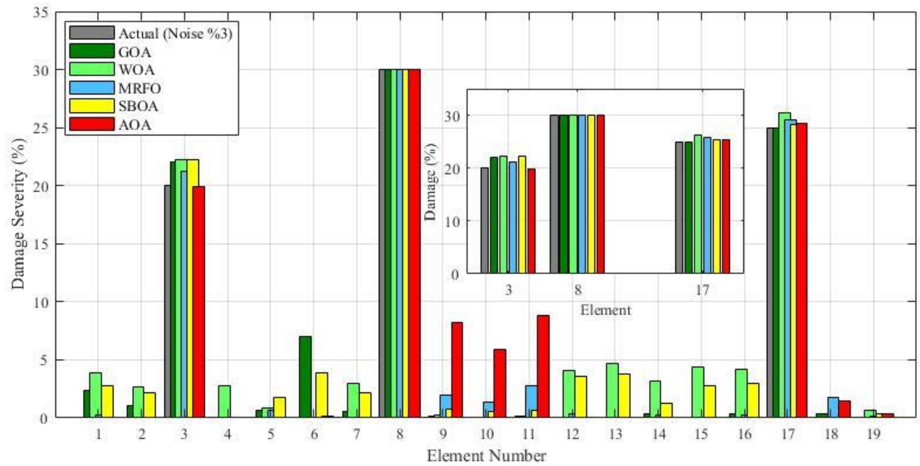

Fig. 26. Damage Identification Results – Scenario 2, 3% Noise (All Algorithms).

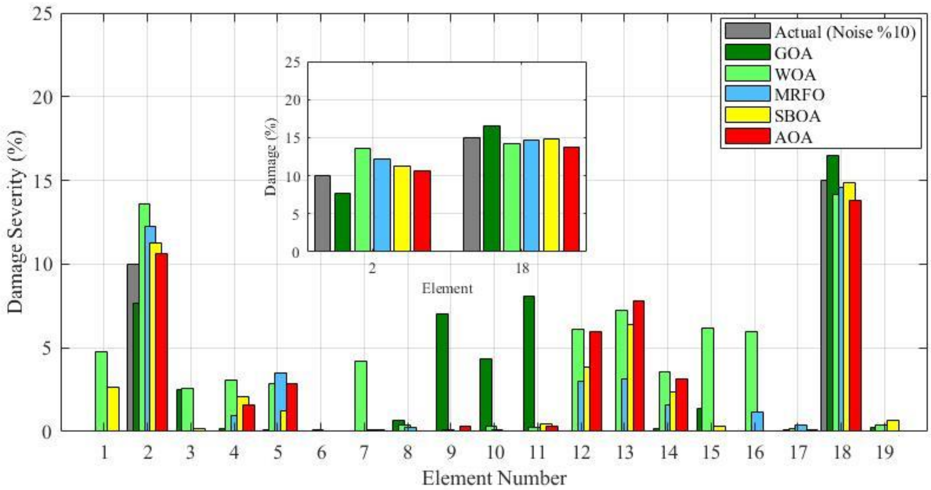

Fig. 27. Damage Identification Results – Scenario 1, 10% Noise (All Algorithms).

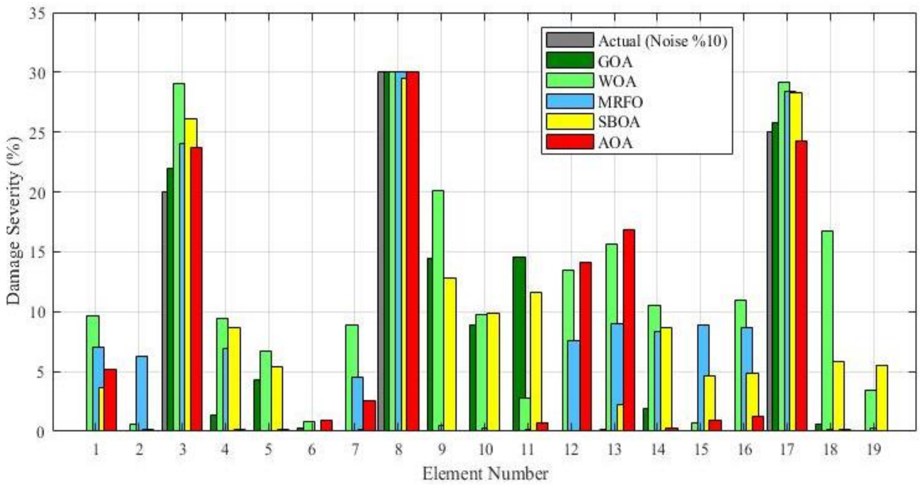

Fig. 28. Damage Identification Results – Scenario 2, 10% Noise (All Algorithms).

The convergence behavior of the algorithms at different noise levels is shown in Figs. 29–31.

Under noise-free conditions, all algorithms effectively minimized the objective function, converging toward values close to zero in both scenarios. In Scenario 1, convergence trends were generally similar across algorithms, indicating stable and consistent performance in simpler damage cases. In Scenario 2, which involved a higher number of damaged members, the convergence behaviors diverged more noticeably. MRFO achieved the most efficient convergence, approaching zero faster and with fewer fluctuations, while SBOA and GOA also converged well though at slightly slower rates. By contrast, AOA exhibited weaker performance, stabilizing at higher objective values and reflecting premature convergence, and WOA demonstrated acceptable results but required more iterations to reach satisfactory levels.

At low noise levels (3%), all algorithms continued to minimize the objective function with acceptable performance, though final convergence values were higher compared to the noise-free cases. In Scenario 1, convergence paths closely resembled those under noise-free conditions, with only slight delays, whereas in Scenario 2 the presence of more damaged members increased variability among algorithms. MRFO and SBOA remained the most effective, converging smoothly with minimal oscillations, while GOA maintained reasonable stability but slightly underestimated convergence precision. WOA exhibited a slower decline, requiring more iterations to reach stable values, and AOA, although convergent, failed to reach an optimal solution, stabilizing at relatively higher objective function values.

At high noise levels (10%), convergence became slower and more irregular, and final objective values increased significantly for all algorithms. Achieving optimal convergence was more challenging, and additional iterations were required to stabilize the solutions. In Scenario 1, GOA and SBOA demonstrated robust performance, showing steady progress toward lower objective values, while MRFO maintained acceptable convergence but was less effective than in lower-noise cases. WOA struggled with slower and less stable convergence, and AOA exhibited the weakest performance, with premature stabilization at high objective values. In Scenario 2, the challenges intensified due to the larger number of damaged elements, amplifying the effect of noise. Here, MRFO and AOA showed substantial performance deterioration, while SBOA preserved better convergence characteristics compared to the others.

Overall, these findings indicate that while all algorithms are capable of converging under different noise conditions, their precision and stability vary significantly. MRFO and SBOA consistently demonstrate stronger noise resistance, GOA performs reliably under moderate noise, whereas WOA and particularly AOA show greater sensitivity, especially in complex damage scenarios with higher noise levels.

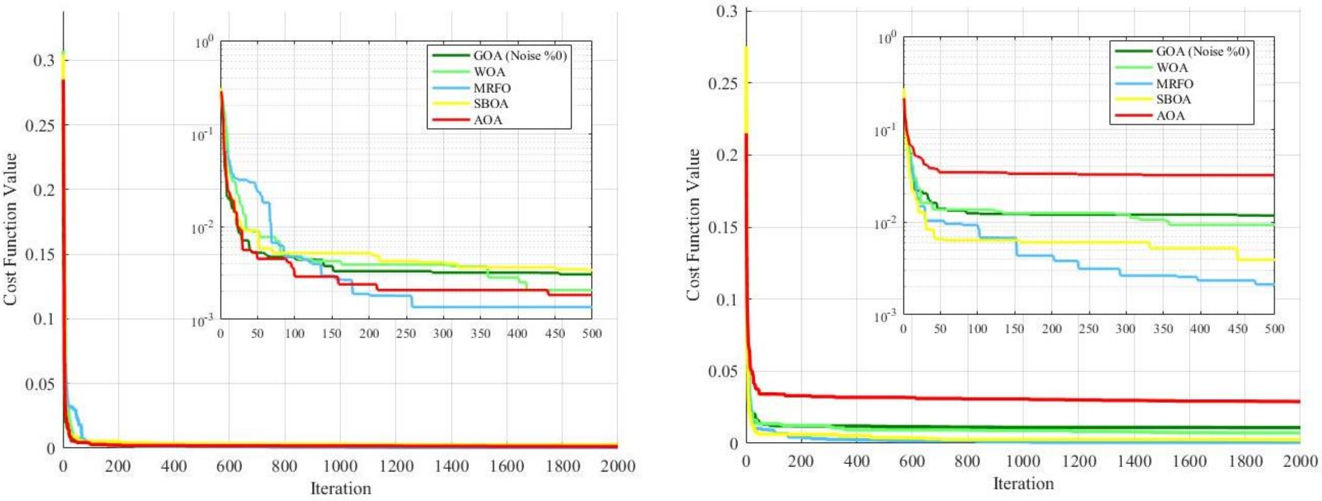

Scenario 1 Scenario 2

Fig. 29. Convergence behavior of all algorithms under noise-free conditions.

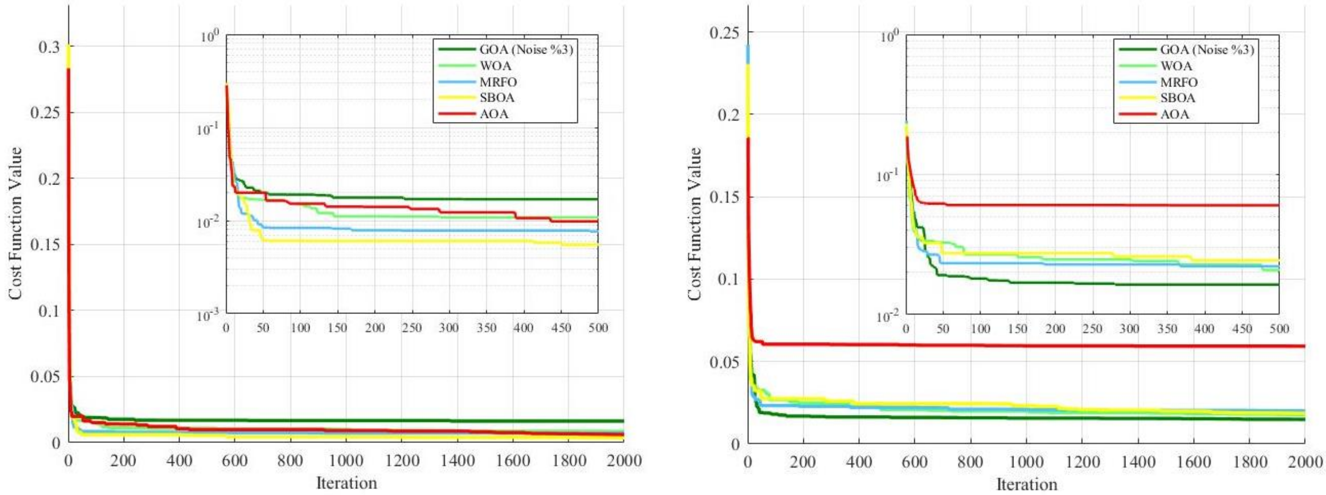

Scenario 1 Scenario 2

Fig. 30. Convergence behavior of all algorithms under 3% noise conditions.

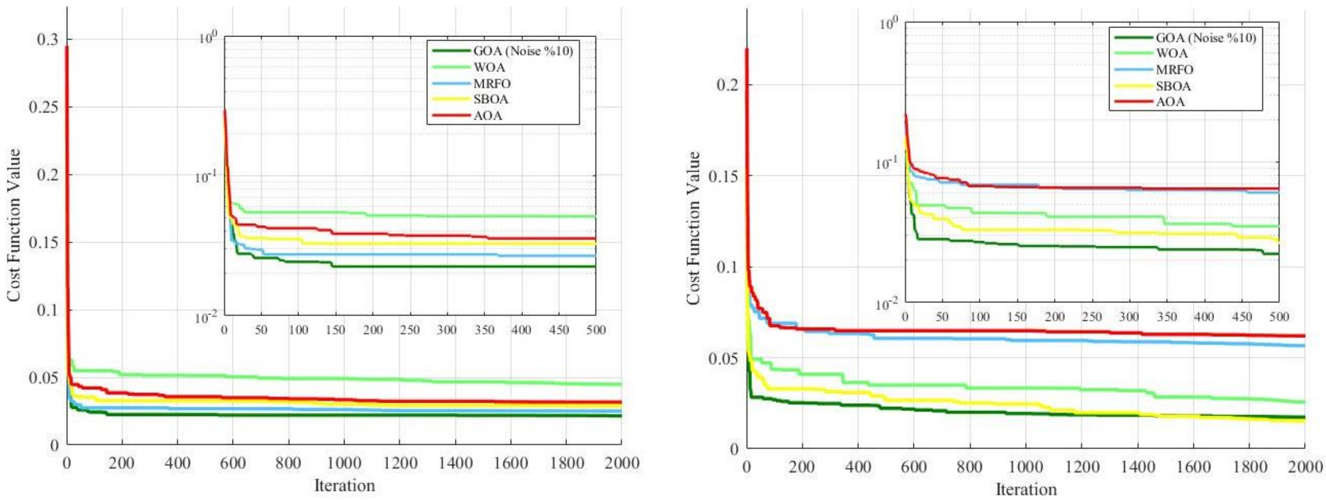

Scenario 1 Scenario 2

Fig. 31. Convergence behavior of all algorithms under 10% noise conditions.

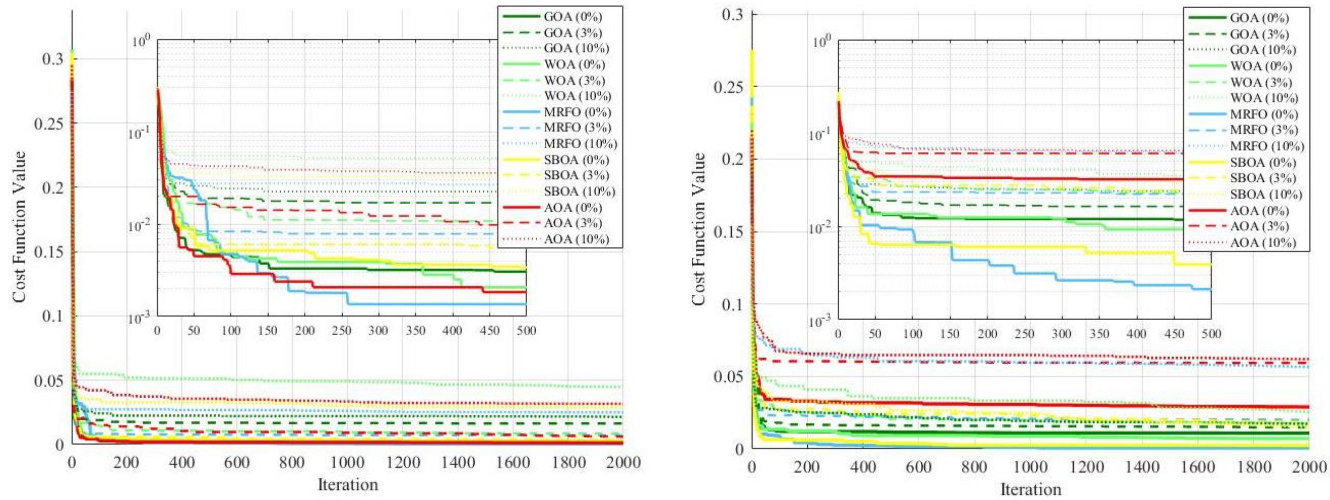

Scenario 1 Scenario 2

Fig. 32. Convergence curves of all algorithms under three noise levels (0%, 3%, and 10%).

Finally, Fig. 32 summarizes the convergence behavior of all algorithms across all three noise levels. The results highlight the disruptive effect of high noise on optimization, leading to increased errors in structural damage identification. Nevertheless, the comparative analysis confirms that MRFO and SBOA consistently provide superior performance, while GOA, WOA, and AOA show greater sensitivity to noise.

6. Hybrid manta-secretary optimization algorithm (MSOA)

The application of metaheuristic optimization algorithms in structural damage detection has received significant attention, as the accuracy of such methods largely depends on the effective optimization of objective functions. However, individual algorithms often struggle to achieve a proper balance between exploration and exploitation or to maintain robustness under noisy conditions. To overcome these limitations, the Manta-Secretary Optimization Algorithm (MSOA) is introduced, integrating the strong exploration capability of MRFO with the precise exploitation ability of SBOA, thereby providing a more accurate and reliable approach for structural damage detection.

MRFO, inspired by the foraging behaviors of manta rays—including chain, cyclone, and somersault strategies—demonstrates strong global exploration and an ability to escape local optima. Its diversified strategies help maintain population diversity and ensure high accuracy in identifying damage locations and severities, even under noisy conditions. However, its exploration dominance may reduce exploitation accuracy and slow convergence in the later stages. Conversely, SBOA, inspired by the secretary bird's hunting strategies, emphasizes local exploitation and achieves rapid convergence to promising solutions. Although robust against noise, its limited population diversity in early stages can restrict global search capability.

By integrating the complementary features of both algorithms, MSOA enhances global exploration in the early and middle iterations while reinforcing precise exploitation in the later stages. The balance is achieved through an adaptive switching mechanism governed by a random probability p and the iteration ratio (ratio = $\frac{t}{T_{max}}$), Accordingly, MRFO operations dominate during early exploration, whereas SBOA mechanisms strengthen exploitation as the algorithm approaches convergence. This adaptive switching makes MSOA particularly suitable for structural damage detection in noisy, high-dimensional environments. The detailed procedure of the MSOA is outlined as follows:

1. Initialize the key parameters, including population size N, maximum number of iterations T_{max}. and the positional boundaries for individuals within the range $[x_{min}\ x_{max}]$. generate the initial population $x_i, i = 1, 2, \ldots, N$.

2. Evaluate the fitness of each individual and identify the best solutions, denoted as $x_{best.MRFO}$ and $x_{best.SBOA}$.

3. Update the population's positions based on the random value p and iteration ratio. If $p > 0.5$, individuals update their positions using SBOA according to C_1 Eq. (37) with $x_{best.SBOA}$. If $p \leq 0.5$ and the iteration ratio is less than 0.5, positions are updated using the MRFO according to Eq. (27), with $x_{best.MRFO}$. Otherwise, if $p \leq 0.5$ and the ratio is at least 0.5, employ the random search mechanism to update positions via SBOA according to C_2 Eq. (37), with $x_{best.SBOA}$.

4. Check if the algorithm meets the convergence criteria or reaches the maximum number of iterations. If either condition is satisfied, terminate the algorithm and return the optimal position x_{best}, otherwise, Otherwise, repeat Steps 2 and 3 for the next iteration.

The following flowchart in Fig. 33. illustrates the MSOA algorithm's steps and switching mechanism.

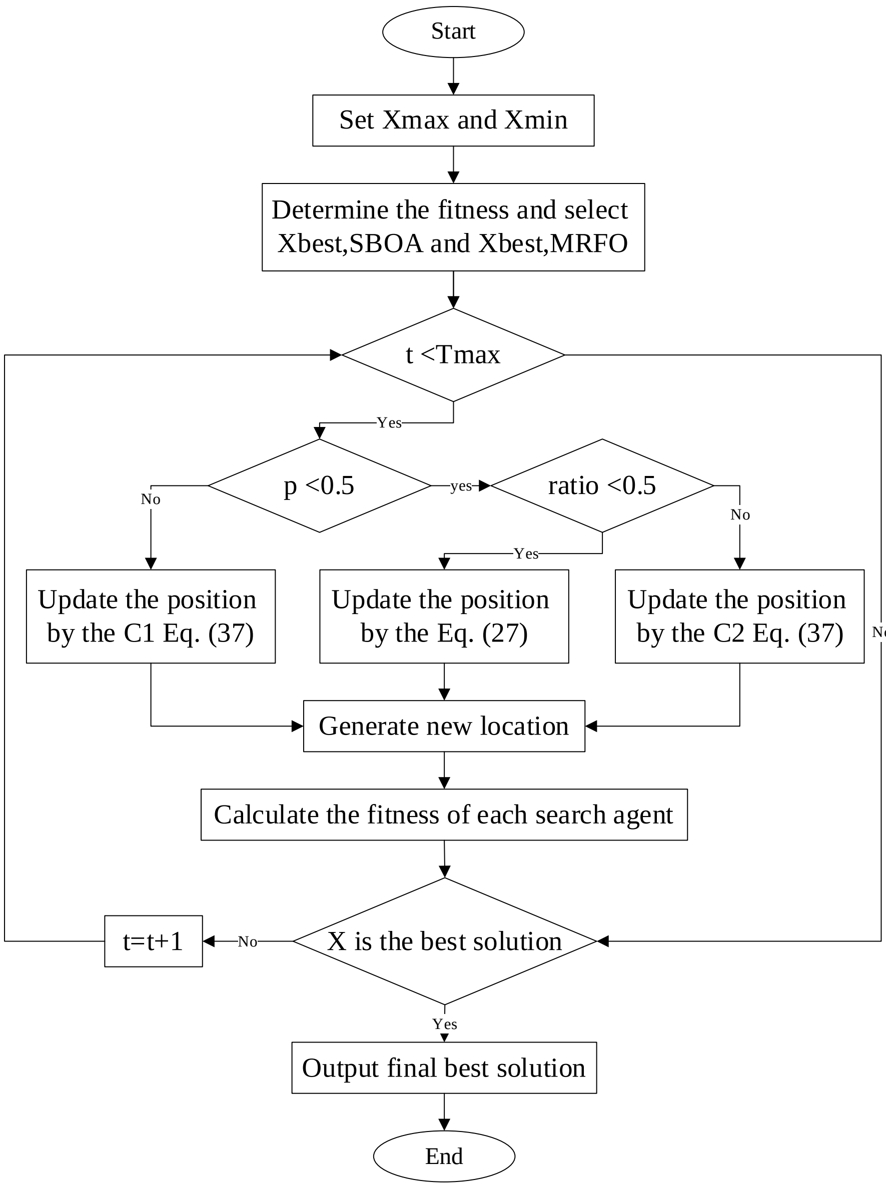

Fig. 33. Flowchart of the MSOA.

6.1. Damage identification results for MSOA

Figures 34 and 35 demonstrate that the proposed objective function, when integrated with the hybrid MSOA algorithm, enables highly accurate identification of both the location and severity of structural damage. This accuracy is maintained under noise-free and low-noise conditions, and even at 10% noise the algorithm remains robust, with only minor misclassifications of undamaged elements reported as slightly damaged. Notably, as the number of damaged elements increases, MSOA further improves its precision, exhibiting enhanced resilience to noise and greater reliability compared to individual algorithms.

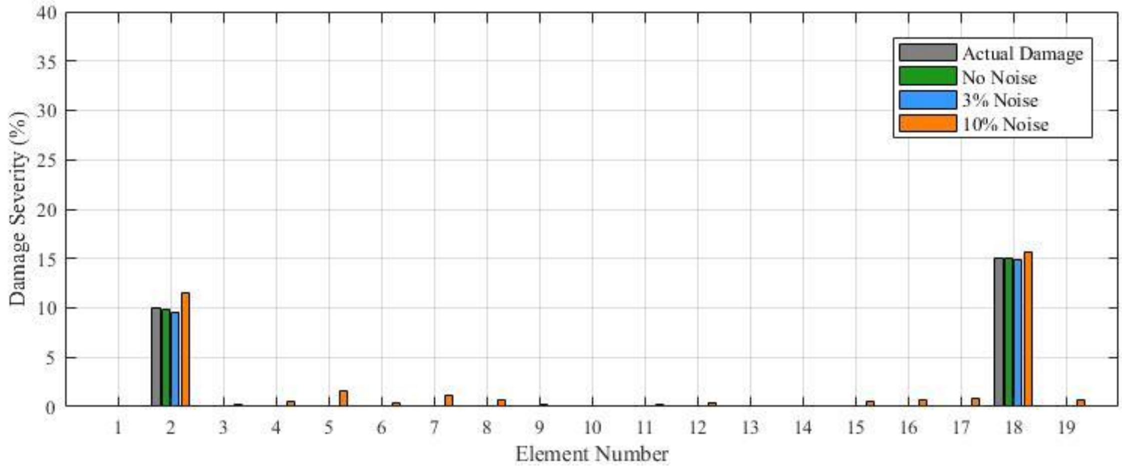

Fig. 34. Identified damage severities for Damage Scenarios 1 under varying noise levels - MSOA.

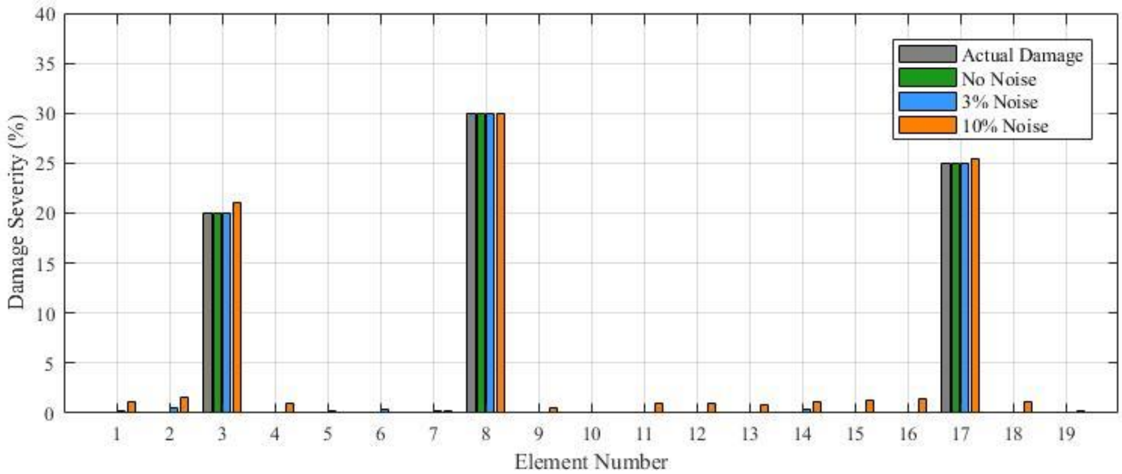

Fig. 35. Identified damage severities for Damage Scenarios 2 under varying noise levels - MSOA.

Figure 36 illustrates the convergence performance of the hybrid MSOA. The objective function decreases rapidly and steadily, converging toward zero with high precision. By combining the exploration capacity of MRFO with the exploitation strength of SBOA, MSOA successfully avoids premature convergence and local optima, ensuring a consistent trajectory toward the global optimum. While noise introduces slight increases in the final objective function value, it does not disrupt the convergence pattern, confirming the robustness and stability of the proposed hybrid framework.

Table 3 presents a comparative summary of six metaheuristic optimization algorithms (GOA, WOA, AOA, SBOA, MRFO, and MSOA) applied to both damage scenarios under different noise levels.

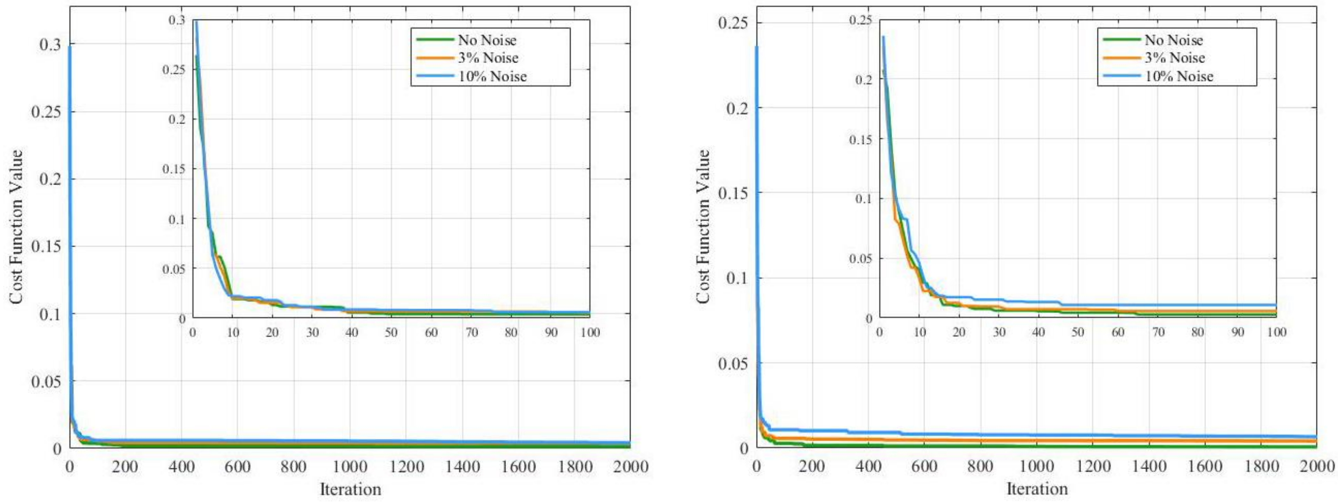

Scenario 1 Scenario 2

Fig. 36. Objective function convergence for Damage Scenario 1 and 2 under varying noise levels - MSOA.

Table 3
Comparative performance of six optimization algorithms in damage detection (Scenario 1 and Scenario 2).

Algorithm	Scenario	Measurement Error (%) (Noise 0% / 3% / 10%)	False Positives (%)	Convergence Rate	Noise Robustness	Damage Localization
GOA	Scen.1	5.44 / 5.81 / 15.35	up to ~15%	Fast	Medium	Good
	Scen.2	1.39 / 2.13 / 2.75	5–14.6%	Fast	Medium	Good
WOA	Scen.1	2.12 / 5.79 / 17.63	up to ~7.2%	Moderate	Weak	Moderate
	Scen.2	1.30 / 3.55 / 13.27	2.4–20.1%	Moderate	Weak	Moderate
AOA	Scen.1	1.87 / 12.52 / 7.39	up to ~7.8%	Slow	Weak	Moderate
	Scen.2	5.10 / 0.55 / 4.46	2.8–16.8%	Slow	Weak	Moderate
SBOA	Scen.1	1.65 / 2.32 / 5.66	up to ~7.4%	Fast	High	Very good
	Scen.2	0.08 / 1.99 / 7.40	up to ~12.8%	Fast	High	Very good
MRFO	Scen.1	0.15 / 2.11 / 10.62	up to ~3.5%	Moderate	High	Very good
	Scen.2	0.23 / 2.50 / 9.93	up to ~8.9%	Moderate	High	Very good
MSOA	Scen.1	0.90 / 2.31 / 6.51	Negligible	Fast	High	Excellent
	Scen.2	0.14 / 0.12 / 2.13	Negligible	Fast	High	Excellent

7. Discussion

This study presented a novel framework for identifying the location and severity of structural damage in moment-resisting frames. The framework employs a model-updating approach based on dynamic characteristics—namely natural frequencies, mode shapes, and modal strain energy—to construct a sensitive and reliable objective function. The performance of five metaheuristic optimization algorithms was assessed, leading to the development of a hybrid algorithm named MSOA. The methodology was tested under two damage scenarios and three noise levels (0%, 3%, and 10%).

The simulation results revealed distinct strengths and weaknesses for each algorithm. MRFO exhibited exceptional accuracy in identifying damage locations and severities under noise-free and low-noise conditions, with stable convergence behavior. SBOA demonstrated reliable performance under high-noise conditions, delivering acceptable precision. GOA, while slightly less accurate in estimating damage severity, showed rapid convergence and strong stability. In contrast, AOA and WOA produced reduced accuracy and a higher number of false positives, particularly at the 10% noise level. Although all algorithms were capable of detecting structural damage, their performance generally declined as the noise level increased.

To leverage the complementary strengths of individual algorithms and overcome challenges related to noise and convergence, the hybrid algorithm MSOA was developed. This method combines the exploratory strength and diversity of MRFO with the exploitation accuracy and stochastic search capabilities of SBOA, regulated by an adaptive switching mechanism based on random probability and iteration ratio. MSOA consistently outperformed standalone algorithms, achieving high damage detection accuracy, stable and rapid convergence, and minimal false positives across all scenarios, even under high-noise conditions.

Despite the promising findings of this study, several limitations must be acknowledged. First, the proposed damage detection framework was developed under the assumption of linear structural behavior and accurate extraction of modal parameters. While this assumption is common in model updating studies, it does not fully capture nonlinear effects such as material nonlinearity, boundary flexibility, and dynamic contact phenomena. Second, the evaluation was conducted under simulated noise levels of up to 10%, which may not encompass the full range of uncertainties present in real measurements.

In addition, the sensitivity of the algorithms to initial conditions and parameter tuning represents a critical limitation. The convergence behavior and final accuracy can be affected by the choice of initial populations as well as by the specific values assigned to control parameters. Although standard parameter settings were adopted in this study to ensure comparability, inappropriate selections may lead to slower convergence or reduced accuracy. Furthermore, the performance of the MSOA algorithm may vary when applied to highly complex optimization problems or under different parameter settings, necessitating further sensitivity analysis and parameter calibration.

Future research could incorporate surrogate models or data-driven machine learning techniques to significantly reduce computational costs and enhance convergence efficiency. Moreover, the framework should be extended to nonlinear and large-scale systems, and its integration with multi-objective optimization strategies and experimental or field data should be explored to improve real-world applicability.

In summary, the proposed framework—featuring a novel objective function and the MSOA algorithm—offers an accurate, noise-resilient, and computationally efficient solution for structural damage detection. The five metaheuristic algorithms demonstrated the effectiveness of the objective function in guiding the optimization process, while MSOA achieved superior convergence and damage detection accuracy across all tested conditions. These findings highlight the potential of the proposed method to advance the field of structural health monitoring.

8. Conclusions

This study introduced a model-updating-based approach for accurately detecting structural damage in moment-resisting frames. A novel objective function was proposed by integrating three key dynamic features—natural frequencies, mode shapes, and modal strain energy—derived from the first three vibration modes. This formulation significantly enhances sensitivity to both global and localized stiffness degradations, enabling reliable damage detection even under noisy conditions.

The effectiveness of the objective function was evaluated using five metaheuristic optimization algorithms: GOA, WOA, MRFO, SBOA, and AOA. These algorithms were tested under two damage scenarios and three noise levels (0%, 3%, and 10%). While all methods demonstrated the capability to detect damage, their accuracy and convergence behaviors varied. MRFO and SBOA exhibited superior robustness under noisy environments, GOA achieved rapid convergence with acceptable accuracy, whereas AOA and WOA showed noticeable performance degradation at higher noise levels.

To address the limitations of individual algorithms and leverage their complementary strengths, a hybrid method named MSOA was developed. MSOA combines the exploratory capacity and diversity enhancement of MRFO with the exploitation accuracy and stochastic search efficiency of SBOA, governed by an adaptive switching mechanism based on random probability and iteration ratio. As a result, MSOA consistently delivered high damage detection accuracy, stable and rapid convergence, and minimal false positives below 1.5% across all tested noise levels.

Simulation results, averaged over 20 independent runs, validated the reliability of the proposed framework. Specifically, MSOA achieved measurement errors of less than 0.5% under noise-free conditions, approximately 2% under 3% noise, and around 4% under 10% noise. These results highlight the strong potential of the proposed method for advancing structural health monitoring by providing an accurate, robust, and computationally efficient solution for structural damage detection.

CRediT authorship contribution statement

Soheil Sabzevari: Conceptualization; Data curation; Formal analysis; Investigation; Methodology; Resources; Software; Validation; Visualization; Writing – original draft; Writing – review & editing.

Hosein Naderpour: Conceptualization; Formal analysis; Investigation; Methodology; Project administration; Supervision; Validation; Writing – review & editing.

Majid Gholhaki: Conceptualization; Formal analysis; Investigation; Methodology; Project administration; Supervision; Validation; Writing – review & editing.

Funding

This research received no external funding.

Conflicts of interest

The author (H. Naderpour) serves as an Editor-in-Chief for Journal of Soft Computing in Civil Engineering. To maintain impartiality and ensure the integrity of the editorial process, the author did not participate in the editorial review or the decision-making process regarding the publication of this article.

References

[1] Afshar A, Nouri G, Ghazvineh S, Hosseini Lavassani SH. Machine-Learning Applications in Structural Response Prediction: A Review. Pract Period Struct Des Constr 2024;29:3124002. https://doi.org/10.1061/PPSCFX.SCENG-1292.

[2] Azimi M, Eslamlou A, Pekcan G. Data-Driven Structural Health Monitoring and Damage Detection through Deep Learning: State-of-the-Art Review. Sensors 2020;20:2778. https://doi.org/10.3390/s20102778.

[3] Mirjalili S, Mirjalili SM, Lewis A. Grey wolf optimizer. Adv Eng Softw 2014;69:46–61.

[4] Mirjalili S. The Ant Lion Optimizer. Adv Eng Softw 2015;83:80–98. https://doi.org/10.1016/j.advengsoft.2015.01.010.

[5] Yamany W, Fawzy M, Tharwat A, Hassanien AE. Moth-flame optimization for training Multi-Layer Perceptrons. 2015 11th Int. Comput. Eng. Conf., IEEE; 2015, p. 267–72. https://doi.org/10.1109/ICENCO.2015.7416360.

[6] Mirjalili S, Lewis A. The Whale Optimization Algorithm. Adv Eng Softw 2016;95:51–67. https://doi.org/10.1016/j.advengsoft.2016.01.008.

[7] Samareh Moosavi SH, Khatibi Bardsiri V. Satin bowerbird optimizer: A new optimization algorithm to optimize ANFIS for software development effort estimation. Eng Appl Artif Intell 2017;60:1–15. https://doi.org/10.1016/j.engappai.2017.01.006.

[8] Fu Y, Liu D, Chen J, He L. Addax Optimization Algorithm: A Novel Nature-Inspired Optimizer for Solving Engineering Applications. Int J Intell Eng Syst 2024;17:732–43. https://doi.org/10.22266/ijies2024.0630.57.

[9] Zhao W, Zhang Z, Wang L. Manta ray foraging optimization: An effective bio-inspired optimizer for engineering applications. Eng Appl Artif Intell 2020;87:103300. https://doi.org/10.1016/j.engappai.2019.103300.

[10] Fu Y, Liu D, Chen J, He L. Secretary bird optimization algorithm: a new metaheuristic for solving global optimization problems. Artif Intell Rev 2024;57:123. https://doi.org/10.1007/s10462-024-10729-y.

[11] Hamadneh T, Kaabneh K, Alssayed O, Eguchi K, Gochhait S, Leonova I, et al. Addax Optimization Algorithm: A Novel Nature-Inspired Optimizer for Solving Engineering Applications. Int J Intell Eng Syst 2024;17:732–43. https://doi.org/10.22266/ijies2024.0630.57.

[12] Liu G, Zhai Y, Leng D, Tian X, Mu W. Research on structural damage detection of offshore platforms based on grouping modal strain energy. Ocean Eng 2017;140:43–9. https://doi.org/10.1016/j.oceaneng.2017.05.021.

[13] Liu G, Zhai Y, Leng D, Tian X, Mu W. Research on structural damage detection of offshore platforms based on grouping modal strain energy. Ocean Eng 2017;140:43–9. https://doi.org/10.1016/j.oceaneng.2017.05.021.

[14] Li XY, Wang LX, Law SS, Nie ZH. Covariance of dynamic strain responses for structural damage detection. Mech Syst Signal Process 2017;95:90–105. https://doi.org/10.1016/j.ymssp.2017.03.020.

[15] Tan ZX, Thambiratnam DP, Chan THT, Abdul Razak H. Detecting damage in steel beams using modal strain energy based damage index and Artificial Neural Network. Eng Fail Anal 2017;79:253–62. https://doi.org/10.1016/j.engfailanal.2017.04.035.

[16] Nabavi S, Gholampour S, Haji MS. Damage detection in frame elements using Grasshopper Optimization Algorithm (GOA) and time-domain responses of the structure. Evol Syst 2022;13:307–18. https://doi.org/10.1007/s12530-021-09389-y.

[17] Nouri Y, Shahabian F, Shariatmadar H, Entezami A. Structural Damage Detection in the Wooden Bridge Using the Fourier Decomposition, Time Series Modeling and Machine Learning Methods. J Soft Comput Civ Eng 2024;8:83–101. https://doi.org/10.22115/scce.2023.401971.1669.

[18] Soleimani Nezhad S, Khademian F, Naderpour H, Kalantari SM, Fakharian P. Signal processing-based damage detection of steel braced frame subjected to consequent excitations. Innov Infrastruct Solut 2024;9:454. https://doi.org/10.1007/s41062-024-01762-5.

[19] Fakharian P, Naderpour H. Damage Severity Quantification Using Wavelet Packet Transform and Peak Picking Method. Pract Period Struct Des Constr 2022;27. https://doi.org/10.1061/(ASCE)SC.1943-5576.0000639.

[20] Du G-F, Bie X-M, Li Z, Guan W-Q. Study on constitutive model of shear performance in panel zone of connections composed of CFSSTCs and steel-concrete composite beams with external diaphragms. Eng Struct 2018;155:178–91. https://doi.org/10.1016/j.engstruct.2017.11.024.

[21] Khatir S, Abdel Wahab M. A computational approach for crack identification in plate structures using XFEM, XIGA, PSO and Jaya algorithm. Theor Appl Fract Mech 2019;103:102240. https://doi.org/10.1016/j.tafmec.2019.102240.

[22] Mehrian SZ, Amrei SAR, Maniat M, Nowruzpour SM. Structural health monitoring using optimising algorithms based on flexibility matrix approach and combination of natural frequencies and mode shapes. Int J Struct Eng 2016;7:398. https://doi.org/10.1504/IJSTRUCTE.2016.079287.

[23] Hoseini Vaez SR, Fallah N. Damage Detection of Thin Plates Using GA-PSO Algorithm Based on Modal Data. Arab J Sci Eng 2017;42:1251–63. https://doi.org/10.1007/s13369-016-2398-6.

[24] Rokhsati M, Mohamadi Dehcheshmeh M, Ghodrati Amiri G, Raissi Dehkordi M. Structural Damage Identification Using Novel Objective Functions and Metaheuristic Algorithms. J Soft Comput Civ Eng 2025;9:95–124. https://doi.org/10.22115/scce.2024.465878.1908.

[25] Huang M, Cheng X, Lei Y. Structural damage identification based on substructure method and improved whale optimization algorithm. J Civ Struct Heal Monit 2021;11:351–80. https://doi.org/10.1007/s13349-020-00456-7.

[26] Nouri Y, Shariatmadar H, Shahabian F. Nonlinearity detection using new signal analysis methods for global health monitoring. Sci Iran 2023;30:845–59. https://doi.org/10.24200/sci.2022.58196.5610.

[27] Sabzevari S, Naderpour H, Gholhaki M. Damage Identification in Moment Frames Using Mode Shape Parameters and IMRFO Algorithm. Civ Infrastruct Res 2025. https://doi.org/10.22091/cer.2025.13741.1648.

[28] Heravi MA, Tavakkoli SM, Entezami A. Structural health monitoring by probability density function of autoregressive-based damage features and fast distance correlation method. J Vib Control 2022;28:2786–802. https://doi.org/10.1177/10775463211020198.

[29] Heravi MA, Naderpour H, Soleimani-Babakamali MH. Unbiased Normalized Ensemble Methodology for Zero-Shot Structural Damage Detection Using Manifold Learning and Reconstruction Error From Variational Autoencoder. Struct Control Heal Monit 2025;2025:8921708. https://doi.org/10.1155/stc/8921708.

[30] Zare Hosseinzadeh A, Ghodrati Amiri G, Jafarian Abyaneh M, Seyed Razzaghi SA, Ghadimi Hamzehkolaei A. Baseline updating method for structural damage identification using modal residual force and grey wolf optimization. Eng Optim 2020;52:549–66. https://doi.org/10.1080/0305215X.2019.1593400.

[31] Chen Z, Yu L. A new structural damage detection strategy of hybrid PSO with Monte Carlo simulations and experimental verifications. Measurement 2018;122:658–69. https://doi.org/10.1016/j.measurement.2018.01.068.

[32] Nguyen-Ngoc L, Tran NH, Bui-Tien T, Mai-Duc A, Abdel Wahab M, X Nguyen H, et al. Damage detection in structures using particle swarm optimization combined with artificial neural network. Smart Struct Syst 2021;28:1–12. https://doi.org/10.12989/sss.2021.28.1.001.

[33] Chen Z, Zhang K, Chan THT, Li X, Zhao S. A Novel Hybrid Whale-Chimp Optimization Algorithm for Structural Damage Detection. Appl Sci 2022;12:9036. https://doi.org/10.3390/app12189036.

[34] Zhang G, Wan C, Yang Z, Xie L, Xue S. Damage detection of civil structures based on hybrid optimization algorithm and combined correlation function of heterogeneous responses. Measurement 2025;246:116678. https://doi.org/10.1016/j.measurement.2025.116678.

[35] Logan DL. A first course in the finite element method. vol. 4. Thomson; 2011.

[36] Chopra AK. Modal Analysis of Linear Dynamic Systems: Physical Interpretation. J Struct Eng 1996;122:517–27. https://doi.org/10.1061/(ASCE)0733-9445(1996)122:5(517).